Pneumococcal attachment to epithelial cells is enhanced by the secreted peptide VP1 via its control of hyaluronic acid processing

Rolando A. Cuevas[1], Elnaz Ebrahimi[1], Ozcan Gazioglu[2], Hasan Yesilkaya[2], N. Luisa Hiller[1*].

1. Department of Biological Sciences, Carnegie Mellon University, Pittsburgh, PA 15213.

2. Department of Respiratory Sciences, University of Leicester, Leicester, United Kingdom.

* Address correspondence to N. Luisa Hiller, lhiller@andrew.cmu.edu

ABSTRACT

The Gram-positive bacterium *Streptococcus pneumoniae* (pneumococcus) is an important human pathogen. It can either asymptomatically colonize the nasopharynx or spread to other tissues to cause mild to severe diseases. Nasopharyngeal colonization is a prerequisite for all pneumococcal diseases. We describe a molecular pathway utilized by pneumococcus to adhere to host cells and promote colonization. We demonstrate that the secreted peptide VP1 enhances pneumococcal attachment to epithelial cells. Transcriptional studies reveal that VP1 triggers the expression of operons involved in the transport and metabolism of hyaluronic acid (HA), a glycosaminoglycan present in the host extracellular matrix. Genetic experiments in the pneumococcus reveal that HA processing locus (HAL) promotes attachment. Further, overexpression of HAL genes in the Δ*vp1* background, reveal that the influence of VP1 on attachment is mediated via its effect on HA. In addition, VP1 also enhances degradation of the HA polymer, in a process that depends on the HAL genes. siRNA experiments to knockdown host HA synthesis support this conclusion. In these knockdown cells, attachment of wild-type pneumococci is decreased, and VP1 and HAL genes no longer contribute to the attachment. Finally, experiments in a murine model of colonization reveal that VP1 and HAL genes are significant contributors to colonization. Our working model, which combines our previous and current work, is that changes in nutrient availability that influence CodY and Rgg144 lead to changes in the levels of VP1. In turn, VP1 controls the expression of a genomic region involved in the transport and metabolism of HA, and these HAL genes promote adherence in an HA-dependent manner. VP1 is encoded by a core gene, which is highly induced *in vivo* and is a major contributor to host adhesion, biofilm development, colonization, and virulence. In conclusion, the VP1 peptide plays a central role in a pathway

32 that connects nutrient availability, population-level signaling, adhesion, biofilm formation,
33 colonization, and virulence.

AUTHOR SUMMARY

Streptococcus pneumoniae (the pneumococcus) is a major human pathogen. This bacterium asymptomatically colonizes the human upper respiratory tract from where it can disseminate to other tissues causing mild to severe disease. Colonization is a prerequisite for dissemination and disease, such that the molecules that control colonization are high-value candidates for therapeutic interventions. Pneumococcal colonization is a population-level response, which requires attachment to host cells and biofilm development. VP1 is a signaling peptide, highly induced in the presence of host cells and *in vivo*, promotes biofilm development, and serves as a potent virulence determinant. In this study, we build on the molecular mechanism of VP1 function to reveal novel bacterial and host molecules that enhance adherence and colonization. Our findings suggest that host hyaluronic acid serves as an anchor for pneumococcal cells, and that genes involved in the transport and metabolism of HA promote adherence. These genes are triggered by VP1, which in turn, is controlled by regulators that respond to nutrient status of the host. Finally, our results are strongly supported by studies in a murine model of colonization. We propose that VP1 serves as a marker for colonization and a target for drug design.

INTRODUCTION

The Gram-positive bacterium *Streptococcus pneumoniae* (also known as the pneumococcus) is an important human pathogen. A recent global study on lower respiratory infections determined that the pneumococcus contributed to morbidity more than all other etiologies combined: it was responsible for an estimated 1.18 million deaths (1,2). This pathogen can either asymptomatically colonize the nasopharynx or spread to other tissues to cause mild to severe diseases. It can spread to the middle ear and sinus, leading to otitis media or sinus infections, and the lungs causing pneumonia (3). It can also disseminate into the bloodstream, brain or heart causing sepsis, meningitis, or heart disease, respectively (4,5). It is well established that nasopharyngeal colonization is a prerequisite for all pneumococcal diseases. In this study, we explore the mechanisms of colonization and virulence.

Pneumococcus secretes many small peptides, which influence colonization, virulence, and adaptation via effects on competence, intra-species competition, and biofilm development (6–18). The **V**irulence **P**eptide 1 (VP1) is a member of a family of peptides with a conserved N-terminal sequence characterized by a double glycine motif, which directs its export into the extracellular milieu via ABC transporters (7,19). The *vp1* gene is widely distributed across pneumococcal strains, as well as encoded in related streptococcal species. The gene encoding VP1 is a virulence determinant and is highly upregulated in the presence of host cells where it promotes biofilm development (7,20). Pneumococcal biofilms have been documented in the nasopharynx, the middle ear, and the sinus (21–24). This mode of growth enhances pneumococcal dissemination and pathogenesis (25,26). Further, biofilms promote pneumococcal colonization in multiple ways: they facilitate immune evasion, increase resistance to antimicrobials, and provide a platform for DNA acquisition (27–29,29–32). In

summary, VP1 is a secreted peptide, induced in the presence of human cells, that promotes biofilm development and virulence.

Glycosaminoglycans (GAGs) are major components of the extracellular matrix. GAGs are acidic linear polysaccharides with a repeated disaccharide unit. The disaccharides consist of an amino sugar (*N*-acetylglucosamine or *N*-acetylgalactosamine) and a uronic acid (glucuronic acid or iduronic acid) or galactose. These polymers are classified into groups based on the nature of the disaccharides, the mode of glycoside bond, and the sulfation levels (33). The main groups are heparin and heparan sulfates (HS), chondroitin and dermatan sulfate (CS), keratan sulfate, and finally hyaluronic acid (HA) (also known as hyaluronate or hyaluronan) (34). Their molecular weights range from 15 to over 100 kDa, and their synthesis takes place in the Golgi apparatus, with the exception of HA, which is synthesized at the membrane (35). GAGs participate in numerous biological processes of the host and the bacteria. In the host, they influence cell adhesion and growth, cell proliferation and differentiation, and tissue formation (for comprehensive reviews, please see Iozzo and Schaefer, 2015; Pomin and Mulloy, 2018; Taylor and Gallo, 2006). In the context of microbial infections, they serve as sources of nutrients and modulators of the immune response (38–41). In addition, many bacteria utilize GAGs to adhere to host cells (42). This includes the pneumococcus, where treatment of lung cells to decrease HS and CS levels reduces pneumococcal adherence (43). In this manner, GAGs are critical components of the bacterial environment during biofilm formation and host interactions.

HA consists of disaccharides of N-acetyl-D-glucosamine (GlcNAc) and D-glucuronic acid (GlcUA). This GAG is present on the apical surface of human bronchial epithelial cells and in the airway mucosa (44,45). It is also abundant in the synovial fluid, skin, umbilical cord, and

vitreous body and is the only non-sulfated glycosaminoglycan in the lung (46–48). This unbranched polysaccharide provides mechanical support, activates immunity, and modulates cell proliferation, migration, and intracellular signaling within the host (49–51). Many streptococcal genomes encode multiple operons for HA transport and metabolism. In the pneumococcus, it has been shown that HA processing and internalization is carried out by a unique set of enzymes including a hyaluronidase, a transporter system, and a hydrolase (52,53). The current model suggests that HA is digested into disaccharides by a hyaluronidase (*hysA* or *hylA*), predicted to be covalently linked to the cell wall via an LPxTG motif. The disaccharides are imported into the bacteria and phosphorylated via a phosphoenolpyruvate-dependent phosphotransferase system (PTS) system. The PTS system is composed of general and substrate-specific components. Enzyme I (EI) and the histidine-containing phosphocarrier protein (HPr) are cytoplasmic subunits, shared by multiple PTS systems. In contrast, Enzyme II (EII) provides specificity to the PTS via substrate recognition. EII has four enzymes: EIIA and EIIB are cytosolic, and EIIC and EIID are the transmembrane components and form a pore. During internalization via the PTS, the HA disaccharides are phosphorylated. These disaccharides are processed by an unsaturated glucuronyl hydrolase (*ugl*) into the monosaccharide components. Finally, the GlcUA can be further processed into glyceraldehyde 3-phosphate and pyruvate by a set of four genes (the isomerase *kduL*, the reductase *kduD*, the kinase *kdgK*, and the aldolase *kdgA*). Operons for the hydrolase, the PTS-EII system, and the GlcUA metabolism enzymes are all adjacent in the genome, and under the control of RegR, a negative regulator located immediately downstream (54). Note that the unsaturated glucuronyl hydrolase not only cleaves HA into GlcNAc and GlcUA, it can also cleave chondroitin sulfate into their component monosaccharides (53,55). The HA pathway has been shown to influence pneumococcal biology. Specifically, *hysA* and the genes in the PTS-EII-

123 encoding operon (EIIB, EIIC, EIID, and *ugl*), are required for pneumococcal growth on human
124 HA, and contribute to pneumococcal biofilm formation and virulence (54,56,57).

125

126 In this study, we show that VP1 promotes pneumococcal adherence via activation of HA
127 transport and metabolism. Our experiments in a murine model of pneumococcal carriage
128 demonstrate that both VP1 and HA processing promote colonization. We propose a model
129 where the nutritional status of the host induces expression of the pneumococcal secreted
130 peptide VP1, via CodY and Rgg144 (7,18,58). Signaling by VP1 triggers HA metabolism in the
131 bacteria, which in turn, regulates attachment to host cells and colonization in the upper
132 airways.

RESULTS

vp1 enhances pneumococcal attachment to epithelial cells

We have previously shown that *vp1* plays a role in biofilm development (7). Thus, we investigated whether *vp1* influences attachment to epithelial cells, an early step in biofilm formation. For these studies, we utilized strain PN4595-T23, a representative of the drug-resistant and pandemic PMEN1 pneumococcal lineage (59–62). To show that the results extend beyond one lineage, we also employed TIGR4, a clinical isolate frequently used as a model strain (63). For host cells, we utilized the human lung epithelial cells line A549. These cells have been extensively used to study pneumococcal behavior (20,64,65). Early works demonstrated that A549 cells display features of type II alveolar pneumocytes: they are capable of surfactant production (66–68), they produce cell surface-associated MUC1 and secrete MUC5AC mucin in air-liquid cultures (69,70), and they produce HA. Further, our experiments on adhesion are extended to NIH-3T3 fibroblasts as they express HA and chinchilla middle ear epithelial cells (CMEE) as these primary cells were used in the original characterization of VP1 function (7,71).

We established that the wild-type strain displays strong attachment to A549 cells after one hour of exposure (Fig S1A). Thus, we used this time point to compare adhesion between wild-type, *vp1* deletion mutant (Δ*vp1*) and *vp1* complement strains (Δ*vp1:vp1*) by using spot plating assays and enumerating the total bound bacteria on TSA plates. The Δ*vp1* displays a reduction in attachment compared to the wild-type cells. Furthermore, the wild-type phenotype is rescued in a *vp1* complement strain (Δ*vp1:vp1*) (Fig 1A). These data suggest that VP1 promotes attachment to the lung epithelia. This role for the *vp1* gene product is not specific to A549 cells, as *vp1* also promotes adherence to chinchilla middle ear epithelial cells (CMEE)

157 and NIH-3T3 fibroblasts (Figs S1B and S1C). Similarly, these results extend beyond the
158 PMEN1 lineage, deletion of the operon encoding *vp1* (*vpo*) in a TIGR4 background also
159 displays decreased attachment relative to the wild-type strain and this phenotype is restored to
160 wild-type levels in a *vpo* complement strain (Fig S1D). Adherent bacteria were visualized by
161 fluorescence microscopy of A549 cells inoculated with PMEN1 cells (Fig 1B). The confocal
162 orthogonal view shows localization at the surface of A549 cells (**Fig S1E**). Finally, the
163 difference in attachment is not the result of variation in growth rate between strains, as growth
164 in DMEM media is the same for wild-type, Δ*vp1,* and Δ*vp1:vp1* strains, as previously reported
165 (7). We conclude that *vp1* promotes pneumococcal attachment to mammalian epithelial cells.

166

167 **The *vp1* product positively regulates expression of HA transport and metabolism genes.**

168 The VP1 pro-peptide possesses a double glycine motif common to secreted peptides
169 that bind surface-bound histidine kinase receptors from pneumococcal two-component signal
170 transduction system (72). Further, synthetic VP1 binds to the pneumococcal surface (7). Thus,
171 we hypothesized that VP1 signals to producing and neighboring cells and induces expression
172 of genes that participate in the attachment.

173

174 To test this hypothesis, we compared the genome-wide expression of the wild-type
175 PN4595-T23 strain and the isogenic Δ*vp1* mutant using the pangenome pneumococcal array
176 (13) (Fig 2A) Strains were grown in chemically defined media (CDM) supplemented with
177 glucose (CDM-Glu), as *vp1* expression is induced in this media relative to rich media (7). In
178 support of the hypothesis, twenty-eight genes displayed a 3-fold difference in expression
179 between the wild-type strain and the Δ*vp1* strain (Fig 2A and S1 Table). Many of these genes

180 are organized into three genomic regions (Fig 2B). Microarray results were validated by qRT-
181 PCR for a subset of genes (S2 Table). Taken together, we observed a significant number of
182 genes with transcription levels that respond to *vp1*.

183

184 Our analysis shows that two neighboring operons display higher expression in the wild-
185 type strain relative to the Δ*vp1;* these operons have been previously implicated in the
186 processing of HA (53). Together, these two operons encode eleven genes that displayed an
187 average 4.28-fold decrease in expression in the Δ*vp1* relative to the wild-type strain (Figs 2B
188 and 3A). One operon is on the positive strand and encodes seven genes. In this study, for
189 simplicity, we refer to this as the PTS-HAL operon as it encodes the four EIIABCD enzymes
190 that form the PTS importer (Fig 3A). This importer is required for phosphorylation and
191 internalization of HA (EII genes are: SPN23F_02950, and SPN23F_02970 to SPN23F_02990).
192 The operon also contains the *ugl* gene that encodes an unsaturated glucuronyl hydrolase
193 (SPN23F_02960), the preprotein translocase YajC that is a subunit of the bacterial holo-
194 translocon (SPN23F_03000) (73), and finally a predicted heparinase (SPN23F_3010). Our
195 analysis with Phyre2 (74), indicates that the heparinase is a glycosidase that belongs to the
196 superfamily of heparinases type II/III; member of this family bind and degrade heparin and
197 heparin sulfate (75). It is noteworthy, that 60 base-pairs downstream of the end of *hep*, is the
198 negative regulator RegR (SPN23F_3020) (76). Analyses of the region upstream of RegR with
199 the promoter identification programs BDPG and BPROM suggests the presence of an active
200 promoter with the -35 within the *hep* sequence (77,78). The second operon regulated by VP1
201 is immediately upstream of the PTS-HAL operon on the negative strand, it encodes four
202 enzymes predicted to metabolize glucuronic acid into glyceraldehyde-3 phosphate and

pyruvate (SPN23F_02910 to SPN23F_02940). These transcriptional findings suggest that *vp1* triggers the expression of genes implicated in the transport and metabolism of HA.

The *vp1* product promotes degradation of the HA polymer via its control of the HA processing and transport operon.

Once we established that VP1 stimulates expression of multiple genes involved in HA metabolism, we tested whether VP1 could influence the processing of the HA polymer. To this end, we measured the hyaluronidase activity in pellets and supernatants of the PN4595-T23 strain carrying deletions of *vp1,* PTS-HAL, and various genes involved in HA processing (Fig 3B). In this assay, bacterial pellets or supernatants were mixed with the HA polymer, degradation of HA was measured as a change in optical density at OD_{400} and reported as hyaluronidase concentration (76). As controls, we employed the Δ*hysA*, as this gene encodes for a hyaluronidase and its deletion should result in reduced hyaluronidase relative to the wild-type strain (53,79). As predicted, this strain displayed 2.6-fold lower hyaluronidase levels ($p < 0.0001$ relative to the wild-type strain). We also employed a Δ*regR* mutant, as this gene encodes for a repressor of *hysA* and its deletion should lead to increased hyaluronidase activity (54). The Δ*regR* strain exhibited elevated hyaluronidase activity ($p = 0.0006$). The Δ*vp1* strain displayed 1.7-fold lower hyaluronidase compared to the wild-type strain ($p < 0.0001$). This defect was rescued in the Δ*vp1:vp1* ($p < 0.0001$ relative to Δ*vp1* strain). The ΔPTS-HAL mutant and the Δ*vp1*-ΔPTS-HAL double mutant showed a 1.4- and 1.5-fold reduction in hyaluronidase relative to the wild-type strain ($p < 0.0005$). This reduction was similar to the Δ*vp1* strain compared to the wild-type strain. The majority of the hyaluronidase activity was captured within the pellets, suggesting that the majority of the degradation enzymes are

226 associated with the cell and not secreted into the supernatant. These data suggest that *vp1*
227 and the PTS-HAL processing and transport operon promote degradation of HA.

228

229 To determine whether the ability to break down HA is conserved beyond the PMEN1
230 strain PN4595-T23, we performed the same set of experiments in a TIGR4 background. The
231 locus in TIGR4 resembles that of the PMEN1 strain, with the addition of a predicted
232 transposon at the end of the operon (see graphic Fig S2A). The results were similar in that the
233 genes encoded by the *vp1* operon (*vpo*) and HA processing and transport operon (PTS-HAL)
234 contributed to the degradation of the HA polymer. In contrast to PN4595-T23, the majority of
235 the TIGR4 activity was localized to the supernatant (Fig S3C), suggesting differences in the
236 subcellular localization of the hyaluronidase activity between strains.

237

238 Finally, to investigate whether VP1 exerts its influence via genes encoded in the HA
239 processing and transport operon, we tested whether overexpression of the PTS-HAL operon in
240 a Δ*vp1* background could rescue the wild-type phenotype in both TIGR4 and PN4595-T23
241 strains. To this end, using the Δ*vp1* backgrounds, we replaced the native promoter of PTS-
242 HAL with a constitutive promoter (from *amiA* gene) (strain Δ*vp1*-OE PTS-HAL)(80). These
243 strains displayed HA degradation comparable to the isogenic wild-type strains (p = 0.21) (Fig
244 3B and S2C). These data suggest that *vp1* exerts its effect on HA metabolism via control of the
245 gene products encoded in the PTS-HAL operon.

246

247 **Pneumococcus attaches to host HA in a process controlled by VP1 and mediated by**
248 **molecules involved in HA processing.**

We have demonstrated that the *vp1* product enhances attachment of pneumococci to lung epithelial cells (Fig 1), and promotes transcription and activity of genes in the HA processing and transport operon associated with HA metabolism (Figs 2 and 3). Thus, we hypothesized that *vp1* influences attachment via its effect on the PTS-HAL operon. To test this hypothesis, we performed attachment assays in a strain with a deletion in the PTS-HAL operon (ΔPTS-HAL); it displayed decreased attachment relative to the wild-type strain (Fig 4A). Moreover, the attachment defect observed in the Δ*vp1* mutant was rescued to wild-type levels in the Δ*vp1*-OE PTS-HAL strain where the genes in the PTS-HAL operon are expressed from a constitutive promoter. These data strongly suggest that the products of *vp1* and PTS-HAL promote adhesion and that the effect of *vp1* is exerted via its influence on PTS-HAL. Further, attachment levels for the double mutant Δ*vp1*ΔPTS-HAL resembled that of the ΔPTS-HAL strain consistent with these gene products acting within the same pathway (Figs S3A and S3B). The Δ*regR* strain, with increased levels of expression for genes encoded in the PTS-HAL operon, resembled wild-type levels. The Δ*hysA* strain displayed similar attachment to the wild-type strain, suggesting that genes in PTS-HAL are not promoting attachment via indirect effects on HysA (Fig S3A). The attachment of the wild-type and mutant strains were also visualized by confocal microscopy, and representative images are displayed in Fig 4B. Together, these data demonstrate that the *vp1* promotes attachment via its control of the genes in the PTS-HAL operon, responsible for processing and transport of HA.

HA production in mammalian cells is controlled by at least three different, membrane-anchored hyaluronan synthases: *HAS1*, *HAS2*, and *HAS3* (35). Previous transcriptomic studies have reported that A549 cells exclusively express *HAS2* and *HAS3*, while *HAS1* remains undetectable (81). Our qPCR analysis corroborates these findings (Fig S3C). To

evaluate whether the HA produced by the A549 cells is implicated in pneumococcal attachment, we employed siRNA to knockdown the expression of *HAS2* and *HAS3* (independently and together) on A549 cells, and 48 h later, assessed the attachment strength of the wild-type strain. As a control for treatment, we used a scrambled construct for siRNA experiments, as well as *HAS1* because it has the low expression levels in A549 (Fig S3C and as described by Chow et al., 2010). At the 48h time point, the siRNA treatment reduced levels of HAS2 and HAS3 to below 20% when compared to the scrambled control (Fig S3D). Our attachment assays revealed a significant reduction in pneumococcal attachment to host cells where HAS2 or HAS3 were knockdown, with maximum reduction in the double knockdown cells (Fig 4C). These data suggest that pneumococcus binding is enhanced in the presence of host HA.

If products of the *vp1* gene and the PTS-HAL operon exert their influence on attachment via HA, a dramatic decrease in host HA levels should reduce the effect of these pneumococcal molecules on host attachment. Consistently, the Δ*vp1* strain displayed similar levels of attachment on host cells independent of the levels of HAS2 HAS3. Further, the ΔPTS-HAL strain also displayed the same levels of attachment in host cells regardless of the levels of HAS2 and HAS3 (Fig 4C). Moreover, attachment of the ΔPTS-HAL strain resembled levels of a wild-type strain on cells with reduced HAS2 and HAS3, that is, substantially lower than attachment to wild type cells. Finally, a strain overexpressing the PTS-HAL operon in the Δ*vp1* background attached better in host cells that express HA. Thus, pneumococcus binding is enhanced by host HA, in a process that depends on the products of *vp1* and PTS-HAL.

296 The influence of HA in promoting pneumococcal binding is further corroborated by an
297 experiment with exogenous HA. In one experiment, the addition of exogenous HA diminishes
298 binding to A549, consistent with bacteria binding to detached HA (Fig S3E). In a second
299 experiment, we coated 6-well plates with HA from *S. equis* (Fig S4A). A spot assay revealed
300 that pneumococcal attachment was substantially higher on a surface coated with HA, relative
301 to those without HA (Fig S4B). As observed on cells, the levels of attachment for Δ*vp1* or
302 ΔPTS-HAL strains were lower than that of the wild-type strain in HA-coated surfaces, and
303 overexpression of the PTS-HAL operon in the Δ*vp1* restored attachment to wild-type levels
304 (Fig 4D). Moreover, these genetic changes had no significant effect on binding on surfaces
305 that were not treated with HA. All together, these data demonstrate that the products of genes
306 involved in the HA processing and transport promote the binding of pneumococcus to host HA
307 in a process regulated by VP1.

308

309 **VP1 and the HA processing and transport operon promote pneumococcal colonization**

310 To establish the role of VP1 and of the PTS-HAL operon in pneumococcal survival in
311 the nasopharynx, we employed the murine model of colonization. Cohorts of five mice were
312 inoculated with single strains, using an inoculation dose of 20μl, where the wild-type strain
313 colonizes the nasopharynx, but not the lungs (83,84). The bacterial load was measured two
314 hours and seven days post-inoculation. Enumeration of pneumococci in the nasopharyngeal
315 lavages two hours post-infection did not show any difference in bacterial load among the
316 strains, indicating the accuracy of infection and the consistency in obtaining nasopharyngeal
317 content (Fig 5A). Throughout the course of infection, the number of recovered wild-type
318 pneumococci remained constant (Figs 5A and 5b).

319

320 Samples recovered seven days post-inoculation revealed significant differences in
321 colony counts across the pneumococcal strains (Fig 5B). Our previous work, in the chinchilla
322 model of pneumococcal disease, established that *vp1* is a virulence determinant based on the
323 reduced mortality and decreased dissemination associated with the *Δvp1* strain relative to the
324 wild-type strain (7). Akin to the chinchilla model, the *Δvp1* strain displayed a dramatic decrease
325 in the murine model, where four out of five animals cleared the infection ($p < 0.0001$).
326 Complementation of *vp1* (Δ*vp1:vp1*) partially rescued the wild-type phenotype. The difference
327 between wild-type and complement (Δ*vp1:vp1*) is likely due to changes in the dose driven by
328 variation of the promoter. These data suggest that VP1 contributes to infection in multiple
329 tissue types, as well as in carriage and disease.

330

331 By the seventh day post-inoculation, we also detected a significant reduction in colony
332 counts in the ΔPTS-HAL and the double Δ*vp1*-ΔPTS-HAL mutants compared to the wild-type
333 strain ($p < 0.0001$). Moreover, overexpression of the PTS-HAL operon in the Δ*vp1* background
334 significantly increased the recovered pneumococci compare to Δ*vp1* ($p < 0.001$). Yet,
335 overexpression of PTS-HAL in the wild-type background had no effect ($p = 0.542$). The
336 observation that the PTS-HAL operon can compensate for the absence of *vp1* is consistent
337 with the model where VP1 acts upstream of HA processing (Figs 5 and 6). These results
338 strongly suggest that VP1 and HA transport and metabolism play a critical role in
339 pneumococcal colonization of the upper airways.

DISCUSSION

The binding of pneumococci to epithelial cells of the host mucosal surfaces is a crucial step during colonization and precedes dissemination to other tissues (3,85,86). In this study, we reveal a pneumococcal pathway that promotes adherence via host HA. We previously documented that the signaling peptide *vp1* is dramatically induced during host infection, enhances biofilm formation, and is a potent virulence determinant in a chinchilla model of middle ear infection (7). Here, we build on this work, providing mechanistic details that reveal links across signaling, adherence, and colonization. Specifically, we demonstrate that VP1 controls genes involved in the transport and metabolism of the host glycosaminoglycan, HA. Our *in vitro* studies demonstrate that genes in the PTS-HAL operon enhance attachment of the pneumococcus to epithelial cells. Our *in vivo* studies on a murine model of colonization suggest that VP1 and the operon for HA transport and metabolism play critical roles in nasopharyngeal colonization.

VP1 is part of a regulatory network involved in nutritional sensing. Previous work demonstrated that the master nutritional regulator CodY negatively regulates the level of vp1 transcripts, and positively regulated by the transcriptional regulator Rgg144 (18,87). The activity of Rgg144 (nomenclature based on gene name in D39, SPD_0144) is regulated by a cognate peptide SHP144 (short hydrophobic peptide 144), which is secreted from cells and internalized into producing and neighboring cells where it binds to Rgg144 (7,18). Rgg144 is a negative regulator of the capsule: it directly binds a predicted promoter upstream of the capsular genes, inhibits the expression of capsular genes, and leads to a reduction in the size of the type 2 capsule (18). The bacterium capsule hinders cell adhesion by concealing bacterial receptors (88). In addition, our work on murine models shows that the Rgg144-

364 SHP144 system serves as a colonization factor in the nasopharynx and contributes to
365 pathogenesis in pneumonia (18). These data are consistent with a model where the Rgg144-
366 SHP144 system plays an essential role in colonization by decreasing the capsule and inducing
367 *vp1*, and that together these events promote adhesion to epithelial cells in the nasopharynx
368 and the lungs. Of note, adhesion experiments in this study were performed in CDM
369 supplemented with glucose. In this condition, levels of *rgg144* are low, and levels of *vp1* are
370 high (7,18). Thus, while Rgg144-SHP144 likely plays a key role in multiple aspects of
371 colonization in our animal model, it is unlikely to be a major contributor *in vitro* experiments
372 presented in this study. We propose that VP1 is a critical component of a complex cellular
373 response to changes in nutritional status.

374

375 Our studies in the murine model of colonization reveal a dramatic defect for the *vp1*
376 deletion mutant, where four out of five mice cleared the infection (Fig 5). The strain with a
377 deletion of the HA transport and metabolism operon also displayed a decrease in bacterial
378 load, but not of the same magnitude as the Δ*vp1*. These data suggest that: (1) VP1 mediates
379 attachment via control of the HA transport and metabolism operon, and (2) VP1 plays
380 additional roles in colonization, which are mediated by yet unknown factors.

381

382 Many pneumococcal surface molecules serve as adhesins, mediating attachment of the
383 bacteria to host cells (40,89,90). A subset of adhesins binds to extracellular matrix
384 components. Pneumococcal virulence protein A and B (PavA and PavB) (91–93) and enolase
385 (94,95) bind to fibronectin and plasminogen. Similarly, the plasmin- and fibronectin-binding
386 proteins A and B (PfbA and PfbB) bind to the extracellular matrix and are required for
387 adherence to lung and laryngeal epithelial cells (96,97). The choline-binding protein A (CbpA

388 or PspC) binds vitronectin (98), and PsrP binds to keratin (99). Pneumococcus also encodes
389 surface-exposed glycosidases, which have been shown to contribute to adhesion not only via
390 modification of the host surface that reveal receptors but also via direct binding (100). The
391 glycosidase NanA (64) and the β-galactosidase BgaA (101), both process GAGs. NanA
392 releases terminal sialic acid residues and BgaA releases terminal galactose residues from
393 glycoconjugates. However, these enzymes promote attachment to host cells in a manner
394 independent of their enzymatic activity. This observation is particularly evident for BgaA, where
395 binding is mediated via a carbohydrate-binding module (102). Thus, the pneumococcal can
396 employ glycosidases in host attachment. In this study, deletion of the surface exposed HysA
397 strongly influenced HA processing (Fig 3), but not attachment (Fig 4). Thus, we deduce that
398 the glycosidase HysA does not mediate the VP1-regulated defect in adhesion.

399

400 The data presented in this study strongly suggest that the transport and processing of
401 host HA plays an essential role in adhesion. However, we have not yet established the
402 molecular mechanism responsible for this outcome. Levels of regulators, carbohydrates, and
403 transporters are interconnected in the bacterial cells via highly complex networks. Regulators
404 control gene expression, including levels of transport systems and biosynthesis enzymes.
405 Carbohydrates can function as substrates, and can positively or negatively influence the
406 activity of regulators. Transporters not only control the import of carbohydrates, but the extent
407 and position of phosphorylated residues on the cytoplasmic Hpr in the PTS system also
408 controls CcpA-dependent carbon catabolite repression (103). CcpA influences the levels of
409 almost one-fifth of pneumococcal genes, including ABC transporters and regulators (103,104).
410 Thus, many molecular mechanisms may explain the connections between transporters and
411 adhesions.

412

413 The HA transport and metabolism locus manipulated in this study encodes all the PTS-
414 EII components (EIIA-EIIB, EIIC, and EIID) that specifically mediate HA import. The locus also
415 encodes two additional genes for a putative heparinase and YajC, a component of the
416 machinery associated with the secretion of proteins with N-terminal signal sequences (73),
417 Data presented in Fig 4, where host HA levels are decreased using SiRNA knockdowns,
418 strongly suggest that the PTS and VP1 mediate attachment, via a yet uncharacterized effector,
419 in an HA-dependent manner.

420

421 Multiple lines of evidence suggest that GAGs facilitate attachment of multiple bacterial
422 species to host cells. Several groups have explored and advanced the utilization of HA to
423 facilitate attachment of bacteria to abiotic surfaces (49,105,106). A recent report showed that
424 multidrug-resistant *Staphylococcus aureus* and *Pseudomonas aeruginosa* form more robust
425 biofilms on surfaces coated with collagen and HA than on uncoated control surface (42). In
426 addition, levels of GAGs on A549 cells were positively associated with the attachment of
427 several pathogens, including *Staphylococcus aureus*, *Streptococcus pyogenes*, and the
428 pneumococcus (43). Similarly, attachment of multiple bacterial species (both Gram-positive
429 and Gram-negative) was positively associated with GAG levels on corneal epithelial cells HCE-
430 2, well known for expressing a variety of GAGs on their surface (40). In yet another example,
431 HA is the primary attachment site of *M. tuberculosis* in A549 cells (107). While HA has not
432 been directly implicated in the attachment of pneumococcus, previous studies demonstrate
433 that the pneumococcus can utilize HA as a carbon source. In particular, *hysA* and genes in the
434 PTS-EII-encoding operon (EIIB, EIIC, EIID, and *ugl*), are required for pneumococcal growth in
435 media where HA is the only carbohydrate (56). Furthermore, HA supports *in vitro*

436 pneumococcal biofilm formation (57). These studies suggest that multiple bacteria may utilize
437 host HA for attachment or nutrients and that control of each or both of these processes
438 influences colonization and virulence.

439

440 In this study, we reveal a novel pathway involved in the attachment of the
441 pneumococcus to host epithelial cells. Our working model is that Rgg144 and CodY monitor
442 nutrient availability and, both of these transcription factors influence levels of the secreted
443 peptide *vp1*. VP1, in turn, controls a genomic region involved in the transport and metabolism
444 of HA, and these genes promote adherence in an HA-dependent manner. VP1 is encoded by a
445 core gene, is highly expressed during infection, and is a significant contributor to both
446 colonization and virulence. Thus, this molecule is a high-value candidate for the development
447 of anti-pneumococcal therapies.

448 # MATERIALS AND METHODS

449 **Bacterial strains and culture conditions.** Wild-type *S. pneumoniae* strain PN4595-T23
450 (GenBank ABXO01), was selected as a representative of the PMEN1 lineage (59–62). The
451 clinical isolate TIGR4 (The Institute for Genomic Research, Aaberge et al., 1995), was
452 graciously provided by Dr. Jason Rosch. The construction of the *vp1* deletion mutant (Δ*vp1*)
453 and the *vp1* complemented strain (Δ*vp1:*Δ*vp1*) in the PN4595-T23 background was reported
454 previously (7). Strain PN4595-T23 was modified to also generate the PTS-HAL operon
455 deletion (ΔPTS-HAL), the *hysA* deletion (Δ*hysA*), and the *regR* deletion (Δ*regR*). We generated
456 a double mutant *vp1*-PTS (Δ*vp1*-ΔPTS-HAL) and a PTS-HAL overexpressor in the Δ*vp1* and
457 wild-type backgrounds (Δ*vp1*-OE PTS-HAL and OE PTS-HAL, respectively) (S5 Table). A
458 similar set of strains was constructed in the TIGR4 background (S5 Table). In this set, we
459 generated a deletion mutant strain of the operon encoding *vp1* (*vpo*) and the *vpo*
460 complemented strain (Δ*vpo*::Δ*vpo*). For growth on solid media, strains were streaked onto
461 Trypticase Soy Agar II plates (TSA) containing 5% sheep blood (BD BBL, New Jersey, USA).
462 For growth in liquid culture, colonies from a frozen stock were grown overnight on TSA plates
463 and inoculated into Columbia broth (Remel Microbiology Products, Thermo Fisher Scientific,
464 USA). The media was supplemented with antibiotics as needed. Cultures were incubated at
465 37°C and 5% CO_2 without shaking. Experiments in chemically defined medium (CDM) were
466 performed utilizing a published recipe (104), and glucose was used at a final concentration of
467 55mM. Growth in CDM was initiated by growing a pre-culture in Columbia broth for 2-3 hours
468 and then diluted to an absorbance of 0.1 at 600 nm, this culture was then grown in CDM-Glu.

469

470 **Strain construction and transformation**. To generate the ΔPTS-HAL mutant strain we used
471 site-directed homologous recombination to replace genes SPN23F_02950 to SPN23F_0310

472 with a kanamycin-resistance gene (*kan*). Likewise, the PTS-HAL operon in the TIGR4 strain
473 (SP_0321 to SP_0327) was replaced with *kan*. The *kan* region was originally amplified from an
474 *rpsL* cassette (80). Gene IDs for PN4595-T23 and TIGR4 are listed in S3 Table. The same
475 strategy was used for the single gene replacements, of *regR* (SPN23F_03020) and *hysA*
476 (SPN23F_02890). To decrease the likelihood of polar effects in all our constructs, the strong
477 artificial transcriptional terminator B1002 was inserted downstream of *kan* (109). Briefly, the
478 transforming DNA was prepared by ligation of the kanamycin gene and promoter, with DNA
479 (one to two kilobases) from the flanking regions upstream and downstream of the PTS-HAL
480 operon. Flanking regions were amplified from the parental strains using either Q5 polymerase
481 or OneTag polymerase (New England Biolabs). The OE PTS-HAL was generated in the Δ*vp1*
482 and wild-type backgrounds by replacing the native PTS operon promoter with an *amiA*
483 promoter and *kan* gene. Assembly of these transforming fragments was achieved by either
484 sticky-end ligation of restriction enzyme-cut PCR products or by Gibson Assembly using
485 NEBuilder HiFi DNA Assembly Cloning Kit. The resulting constructs were transformed into
486 PN4595-T23 or TIGR4. Primers used to generate the constructs are listed in S4 Table.
487 PN4595-T23 and TIGR4 strains were transformed with approximately 1 μg of DNA. Liquid
488 cultures were supplemented with 125 μg ml^{-1} of CSP1 (EMRLSKFFRDFILQRKK, for TIGR4) or
489 CSP2 (EMRISRIILDFLFLRKK, for PN4595-T23), at an absorbance of 0.05 at 600 nm
490 (GenScript, NJ, USA), and incubated at 37°C. After 2 hours, the treated cultures were plated
491 on Columbia agar containing the appropriate concentration of antibiotic for selection,
492 spectinomycin, 100 μg ml^{-1}, kanamycin 150 μg ml^{-1}). Resistant colonies were cultured in
493 Columbia broth. Sequences were confirmed using DNA sequencing of the PCR amplimers
494 (Genewiz, Inc., USA). All strains generated in this study are listed in S5 Table.

495

496 **RNA purification, reverse transcription (RT) and qPCR.** Bacterial samples were collected
497 on RNALater (Thermofisher), and pellets were lysed with 1x lysis mix containing 2 mg ml^{-1} of
498 proteinase K, 10 mg ml^{-1} of lysozyme, and 20 µg ml^{-1} mutanolysin in TE buffer (10 mM Tris·Cl,
499 1 mM EDTA, pH 8.0) for 20 min. Total RNA was isolated using the RNeasy (Zymo Research)
500 following manufacturer instructions. Contaminant DNA was removed by incubating total RNA
501 samples with DNase (2U/µl) at 37°C for at least 15 min and then checked by amplification of
502 *gapdh* (no visible band should be observable in RNA only samples). RT reaction was
503 performed using 1 µg of total RNA using SuperscriptVILO kit for 1 h. Five ng of total cDNA was
504 subjected to real-time PCR using PowerUp SYBR Green Master Mix in the ABI 7300 Real-
505 Time PCR system (Applied Biosystems) according to the manufacturer's instructions. All qRT-
506 PCR amplification was normalized to pneumococcal *gapdh* and expressed as fold change with
507 respect to the wild-type strain. qPCR primers are listed in S4 Table. Primers were obtained
508 from IDT (Integrated DNA Technologies).

509

510 **Spot assays and CFU counts**. Bacteria were inoculated from overnight plates into 20 ml of
511 Columbia broth. Liquid cultures were grown statically and monitored at an optical density of
512 600 nm using Nanodrop 2000c spectrophotometer (Thermo Scientific). Bacterial counts were
513 assessed by streaking 10-fold dilutions on TSA or TSA-antibiotic containing plates. Spot
514 assays were performed with 5 µl of ten-fold dilutions.

515

516 **Microarray Analysis:** We utilized the Pneumococcal Supragenome Hybridization Array
517 (SpSGH) to compare gene expression between the wild-type PN4595-T23 strain and the Δ*vp1*
518 as described previously (13). Pneumococcal cultures were collected and normalized to an
519 absorbance of 0.3 at 600 nm. RNA extraction, cDNA preparation, and cDNA labeling were

performed as described previously (110). Cyber T was used for data analysis (111). Microarray experiments were performed in triplicate. Genes with at least a 3-fold difference between strains and a Bayesian *p*-value < 0.05 were selected for further analysis. Microarray data for selected genes was confirmed by qPCR.

Preparation of HA-coated surfaces. Hyaluronic acid from *Streptococcus equi* (Sigma-Aldrich) was bound to tissue culture 24-wells plates following a previously described method with modifications (49). Briefly, twenty-four well plates (VWR) were treated with 0.5 ml of concentrated sulfuric acid for 10 min at 60°C, washed extensively with distilled water, then incubated for 2 h at 37°C with 0.5 ml 5 mg ml^{-1} of hyaluronic acid. Finally, the plates were rinsed with distilled water and allowed to stand for 1h at room temperature. Plates were not dried during the entire procedure. Control plates were treated solely with either sulfuric acid or HA alone. Hyaluronic acid binding was assessed with 0.5 ml of 1% of Alcian Blue 8GX (Sigma-Aldrich) for 10 min at room temperature, then washed extensively with distilled water.

Hyaluronidase activity measurement. Hyaluronidase activity was measured as described previously (76,112). Briefly, pneumococcal cultures were grown in Columbia broth to an absorbance of 0.7 at 600 nm. Then the bacterial pellet and supernatant were obtained by centrifugation. Prior to the reaction, bacterial pellets were washed thoroughly with PBS at room temperature then diluted in 250 µl of assay buffer while supernatant samples were diluted 1:1 in assay buffer. Hyaluronic acid isolated from *Streptococcus equi* (Sigma Aldrich) was utilized at a final concentration of 10 ug ml^{-1} in assay buffer (150 mM NaCl, 200 mM sodium acetate, pH 6) for 15 min at 37°C. Stop buffer (2% NaOH, 2.5% cetrimide) was added to stop the reaction, and the absorbance at 400 nm was determined. Commercial hyaluronidase from

544 bovine testes (Sigma-Aldrich) was used as positive control. Assay results were calculated
545 using the standard curve from the positive controls and by comparison to that of a blank
546 comprised of assay buffer solely or without bacterial material.

547

548 **Mammalian cells and media growth conditions.** Epithelial lung human carcinoma A549 and
549 fibroblast NIH-3T3 cells were propagated and maintained at 37ºC and supplemented of 5%
550 carbon dioxide at pH 7 in DMEM media contained 1% L-glutamine, 5% fetal bovine serum
551 (FBS) without antibiotics. Chinchilla middle ear CMEE cells were maintained as previously
552 reported (7,71).

553

554 **siRNA knockdown**. All transfection reagents were provided by Sigma-Aldrich. Subconfluent
555 A549 cultures (20% to 30%) were seed in 24-wells plates and transfected with 3 pmol of a
556 mixture containing pre-designed siRNA. Each mixture consisted of multiple siRNA targeting
557 specifically either *HAS1*, *HAS2*, and *HAS3*. Universal control siRNA was used as a negative
558 control. siRNA was transfected in a final volume of 100 μl of OptiMEM containing 3 μl of
559 MISSION siRNA transfection reagent and no antibiotics. Twenty-four hours later the medium
560 was replaced by DMEM supplemented with fetal bovine serum (FBS). Forty-eight hours after
561 transfection, cells were used in adherence assays. To verify the reduction in *HAS* expression,
562 A549 cells were lysed using the RNeasy kit and relative *HAS1*, *HAS2*, *HAS3*, and *ACTINB*
563 expression was verified by qPCR, as described above.

564

565 **Pneumococcal host cell adherence assay.** A549, NIH-3T3 or CMEE were seed in 24-wells
566 plates or on Lab-Tek II Chamber Slides (Thermo Fisher) at a density of 1 x 10^5, and

maintained without antibiotic until confluence. Before infection, the cell monolayer medium is replaced with fresh medium and then infected with pneumococci resuspended in DMEM supplemented with 1% FBS using a multiplicity of infection (MOI) of 50 bacteria per cell. Infected cells were incubated at 37°C in 5% CO_2 for 1 h. Then the media of post-infected cells was aspirated and washed thoroughly three times with PBS to remove unbound bacteria. The total number of adherent bacteria was released with saponin (1% w/v) for 15 minutes at 37 °C and plated on TSA plates followed by colony formation and enumeration. The effect of exogenous HA on attachment interference was performed through the addition of HA from *Streptococcus equi* at concentrations ranging between 0.01 to 1 mg/ml to the A549 monolayers before the addition of the bacteria. Each experiment was repeated at least four times, and results were expressed as mean ± S.E.M.

Confocal microscopy. A549 cells were seeded on Nunc Lab-Tek 4-chamber (VWR) and inoculated with pneumococcal strains with a MOI of 50 as described above. After 1 hour of infection, cells were washed 3-times with PBS and fixed with 4% PFA, washed with PBS and stained with BODIPY FL Vancomycin (Thermo Fisher Scientific), Alexa Fluor 568-Phallodin (Thermo Fisher Scientific) following manufacturer's instructions. Finally, cells were covered with Vectashield mounting media with DAPI (Vector Laboratories). Confocal microscopy was performed on the stage of Carl Zeiss LSM-880 META FCS, using 488 nm laser line for the fluorescence tag and 561 nm laser line for the fluorescence Alexa tag. Images were analyzed using ZEN Black software (Carl Zeiss Microscopy, Thornwood, NY) and assembled in Fiji (ImageJ. 2.0.0rc48). Laser intensity and gain were kept the same for all stacks and images.

590 ***In vivo* studies**: Colonization ability of pneumococcal strains were tested essentially as
591 previously described (83,84). Nine-week-old CD1 mice were raised in the pre-clinical facility of
592 the Leicester University. Mice were anesthetized lightly with 2.5% isoflurane over oxygen (1.5
593 to 2 liter/min), and they were inoculated intranasally with 20 μl PBS, pH 7.0, containing
594 approximately $5X10^5$ CFU/mouse. When inoculating, mice were kept horizontally to prevent the
595 dissemination of inoculum into the lower respiratory tract. A group of mice (n = 5) for each
596 cohort were killed by cervical dislocation at 2 hours and 7 days after infection. After removing
597 the mandible, nasopharyngeal cavity was accessed using a 18G needle through the soft
598 palate, and the content of nasopharynx was collected by injecting 500 μl PBS, pH 7.0. This
599 process was repeated once more using the same lavage fluid in order to optimize the recovery
600 of bacteria. Undiluted and serially diluted lavage fluid was plated on blood agar base plates
601 and CFU/nasopharynx was calculated. The results were analyzed by two-way ANOVA
602 followed by Tukey's multiple comparisons test.

603

604 **Ethics statement:** Mouse experiments were done under the UK Home Office approved
605 project (permit no: P7B01C07A) and personal (permit no. I66A9D84D) licenses. The protocols
606 used were approved by both the UK Home Office and the University of Leicester ethics
607 committee. We used anesthetic during the procedure to minimize the suffering. Moreover, the
608 animals were kept in individually ventilated cages, had access to water and feed *ad libido*, and
609 their health were checked regularly in accordance with the legal and institutional requirements.

610

611 **Statistical analysis.** Statistical significance was assessed using Student's two-tailed *t*-test for
612 independent samples, one-way ANOVA and Bonferroni's multiple comparisons test for

613 independent samples, and two-way ANOVA and Tukey's multiple comparisons test for animal

614 data. *p*-values less than 0.05 were considered statistically significant.

Acknowledgments

We are very grateful to Dr. Aaron Mitchell and Dr. Frederick Lanni for their insightful suggestions and guidance during this project. We also thank Dr. Samantha King for productive discussions, particularly in regards to hyaluronic acid. We thank Dr. Haibing Teng from the Molecular Biosensor and Imaging Facility (MBIC) at Carnegie Mellon University for her assistance with confocal imaging. We thank Dr. Phil G. Campbell for providing A549 cells. This work was supported by NIH grant R01 AI139077-01A1 to N.L.H., the Eberly Family Career Development Professorship of Biological Science, an award from the Samuel and Emma Winters Foundation, as well as support from Carnegie Mellon University. The authors declare that there are no conflicts of interest.

Author Contributions

RAC contributed to the conception, design, experimentation, analysis and interpretation, and manuscript preparation; EE contributed with design and construction of bacterial clones, as well as data interpretation; OG contributed with *in vivo* experiments and data analysis, HY contributed with *in vivo* experiments, analysis and interpretation, and manuscript preparation; NLH contributed design, analysis and interpretation, and manuscript preparation.

Figure Captions

Fig 1. *vp1* enhances pneumococcal attachment to epithelial cells.

(A) A549 lung epithelial cells were exposed to the wild-type PMEN1 strain PN4595-T23, and isogenic *vp1* mutant and *vp1* complemented strains (Δ*vp1* and the Δ*vp1:vp1,* respectively) for 1h at 37 °C. After washing the unbound bacteria, the remaining cell-bound bacteria were recovered and quantified on TSA plates. Visualization by a spot assay performed with 5 µl of ten-fold dilutions (top panel). Quantification of the total number of bacteria bound to epithelial cells based on counts from TSA plates (bottom panel). (B) Representative image of wild-type and the Δ*vp1* strains bound to A549 cells. Bacterial cells were stained with BODYPI-FL vancomycin (green), actin was visualized with TRITC-phalloidin (red), and bacterial and host DNA were visualized with DAPI (blue). Data on A represents the mean ± S.E.M of at least six independent experiments. Statistical significance was calculated using unpaired one-way ANOVA analysis with Bonferroni correction, and multiple comparison between samples were performed. * $p < 0.0001$, ns = not significant with $p = 0.080$.

Fig 2. The *vp1* product positively regulates the expression of an operon critical to processing of hyaluronic acid.

(A) Microarray transcriptome analysis comparing the expression profiles of the wild-type PMEN1 strain PN4595-T23 and *vp1* derivative strain (Δ*vp1*) on CDM supplemented with glucose. Data was analyzed for statistical significance using CyberT as per Student's T-test. The dashed blue lines represent 4-fold up- and down-regulation, respectively. The red circle highlights genes associated with hyaluronic acid metabolism. (B) Selected genomic regions with 3-fold difference in expression between the wild-type and the Δ*vp1* strains. Targets were

655 sorted by their genomic position on the genome. Operons are indicated by brackets. Color
656 code illustrates expression ratio between the Δ*vp1* strain relative to wild-type strain. Gene IDs
657 correspond to those in PMEN1 reference strain ATCC700669 (GenBank FM211187), and the
658 predicted functions based on Pfam. Full set presented in S1 Table.

659

660 **Fig 3. The *vp1* product promotes degradation of the hyaluronan polymer via its controls**
661 **of the operon encoding the PTS-EII system.**

662 (A) Schematic of the genomic region implicated in the metabolism of hyaluronic acid. Arrows
663 correspond to predicted open reading frames. Black and white denote predicted operons. Grey
664 corresponds to genes involved in HA metabolism, but not highly controlled by *vp1*. The IDs
665 refer to gene names in the PMEN1 reference strain ATCC700669. (B and C). Measurements
666 of breakdown of hyaluronan and isogenic deletion mutants for *vp1* (Δ*vp1*), the hyaluronic acid
667 locus PTS operon (ΔPTS-HAL), *vp1* and the PTS operon (Δ*vp1*-ΔPTS-HAL), *hysA (Δhys)*, and
668 *regR* (Δ*regR*), and for a *vp1* complemented strains (Δ*vp1:vp1*), and a PTS overexpressor in
669 the Δ*vp1* background (Δ*vp1*-OE PTS-HAL). Both the pellets (B) and the supernatants (C) of
670 bacteria grown in liquid cultures were collected and assessed for hyaluronidase activity. Data
671 on B and C represents the mean ± S.E.M of at least six independent experiments. Statistical
672 significance was calculated using unpaired one-way ANOVA analysis with Bonferroni
673 correction, and multiple comparison between samples were performed. * $p < 0.05$, ** $p <$
674 0.001, ns = not significant relative to the wild-type strain. Note that on B, the complemented
675 Δ*vp1:vp1* rescues the hyaluronidase deficiency of the Δ*vp1* mutant ($p < 0.0001$) and the
676 overexpressor Δ*vp1*-OE PTS-HAL rescues the hyaluronidase activity of the mutants Δ*vp1* ($p <$
677 0.0001). Further, there is no significant difference between Δ*vp1* and ΔPTS-HAL, between
678 Δ*vp1* and Δ*vp1*-ΔPTS-HAL.

Fig 4. Pneumococcus attaches to host HA in a process controlled by VP1 and mediated by molecules involved in HA processing.

(A) The wild-type PN4595-T23, Δ*vp1*, ΔPTS-HAL, and Δ*vp1*-OE PTS-HAL strains were tested for attachment to epithelial A549 cells. Cell bound bacteria were enumerated by plating on TSA plates. (B) Representative image of strains attached to epithelial A549 cells. Bacterial cells were stained with BODYPI-FL vancomycin (green), actin was visualized with TRITC-phalloidin (red), and DNA was visualized with DAPI (blue). (C) Adherence measurements on A549 cells. *HAS1-, HAS2-,* and *HAS3*-knockdown, and the double-knockdown of *HAS2* and *HAS3* (HAS2-3) cells were exposed to wild-type and its derivative Δ*vp1*, ΔPTS-HAL, and Δ*vp1*-OE PTS-HAL strains. siRNA treatment was administered 48 h before addition of bacteria, and adherent bacteria were enumerated by plating on TSA plates. Bound bacteria were enumerated by plating cells on TSA plates. (D) The wild-type PN4595-T23 and its derivative Δ*vp1*, ΔPTS-HAL, and Δ*vp1*-OE PTS-HAL strains were assessed for attachment to hyaluronic acid-coated surfaces in FBS-supplemented DMEM media. The total cell-bound bacteria were recovered and quantified by growth on TSA plates. Data on A, C, and D represents the mean ± S.E.M of at least four independent experiments. Statistical significance was calculated using unpaired one-way ANOVA (A and D) or two-ways ANOVA (C) analysis with Bonferroni correction, and multiple comparison between samples were performed. * $p < 0.05$, **** $p < 0.0001$, ns = not significant. Note that the overexpressor Δ*vp1*-OE PTS-HAL rescues the attachment deficiency of the mutant Δ*vp1* ($p < 0.0001$) in D.

Fig 5. HA processing region is required for pneumococcal colonization.

CD1 mice were inoculated intranasally with 20 ml PBS containing approximately $5X10^5$ CFU/mouse. At 2 hours (day 0, A), and 7-days (B) post inoculation, nasopharyngeal contents were collected and pneumococci were enumerated. Each column represents the mean of data from five mice. Error bars show the standard error of the mean. Significant differences in bacterial counts are seen comparing to the wild-type strain using two-way ANOVA and Tukey's multiple comparisons test. * $p < 0.0005$, ns = not significant. Note that at day 7, the complemented Δ*vp1:vp1* rescues the colonization deficiency of the Δ*vp1* mutant ($p = 0.003$). Similarly, the overexpressor OE PTS-HAL rescues the colonization deficiency of the mutants Δ*vp1* ($p < 0.0001$). The ΔPTS-HAL ($p = 0.0001$) and the double-mutant Δ*vp1*-ΔPTS-HAL ($p = 0.0001$) both are significantly different from the wild-type strain and the colonization deficiency in the Δ*vp1* strain is greater to the ΔPTS strain (p = 0.0176).

Fig 6. Working model for VP1 regulation and its role in cell-cell communication in *Streptococcus pneumoniae*.

The VP1 is processed and secreted into the extracellular milieu. *vp1* is highly upregulated in the presence of host cells and is induced by an upstream transcription factor, Rgg/Shp. In addition, previous work shows that levels of *vp1* respond to nutrients and to the master regulator CodY. VP1 induces changes in the expression of multiple operons, including two implicated in the processing and acquisition of hyaluronic acid. We propose that VP1 promotes attachment via its influence on the products of genes encoded in the PTS-HAL operon.

Fig S1. *vp1* enhances pneumococcal attachment to epithelial cells.

(A) A549 cells were inoculated with the wild-type PMEN1 strain PN4595-T23. After washing the unbound bacteria, the total cell-bound bacteria were recovered. For visualization, five microliters of ten-fold dilutions were used for spot assays on TSA plates (left panel). For quantification, the total number of bacteria was determined by enumeration on TSA plates (right panel). (B and C). Attachment assay were performed on CMEE cells (B) and NIH-3T3 cells (C) inoculated with the strain wild-type PN4595-T23, the *vp1* mutant and *vp1* overexpressor strain (Δ*vp1* and the Δ*vp1:vp1,* respectively). As in A, cell-bound bacteria were recovered and enumerated on TSA plates (bottom panels). (D) A549 cells were inoculated with the wild-type TIGR4 strain and its derivative *vpo* mutant and *vpo* overexpressor strains (Δ*vpo* and the Δ*vpo::vpo,* respectively). The total cell-bound bacteria were recovered and enumerated as in A. (E) Representative orthogonal view image of A549 cells inoculated with wild-type PN4595-T23. Note the extracellular *foci* indicating surface binding of the bacteria. Bacterial cells were stained with BODYPI-FL vancomycin (green), actin was visualized with TRITC-phalloidin (red), and bacterial and human DNA was visualized with DAPI (blue). Data on A, B, C, and D represents the mean ± S.E.M of at least four independent experiments. Statistical significance was calculated using unpaired one-way ANOVA analysis with Bonferroni correction, and multiple comparison between samples were performed. * $p < 0.005$, ** $p < 0.001$, *** $p < 0.0001$, ns = not significant.

Fig S2. The *vp1* product promotes degradation of the hyaluronan polymer via its controls of the operon encoding the PTS-EII system in TIGR4.

(A) Schematic of the genomic region implicated in the metabolism of hyaluronic acid. Arrows correspond to predicted open reading frames in TIGR4. Black and white denote predicted operons; PTS-HAL has two additional open reading frames at the end of the predicted operon

(represented in white). Grey corresponds to genes involved in HA metabolism, but not highly controlled by *vp1*. The IDs refer to gene names in the TIGR4 genome. (B and C) Measurements of breakdown of hyaluronan by strain TIGR4 and isogenic mutants. Both the supernatants (B) and the pellets (C) of bacteria grown in liquid cultures were collected and assessed for hyaluronidase activity relative to the wild-type strain. Data on B and C represents the mean ± S.E.M of 8 independent experiments. Statistical significance was calculated using unpaired one-way ANOVA analysis with Bonferroni correction, and multiple comparison between samples were performed. * $p < 0.05$, ** $p < 0.05$, *** $p < 0.0001$ ns = not significant relative to the wild-type strain. Note that on C, the Δ*vpo:vpo* rescues the hyaluronidase deficiency of the Δ*vpo* mutant ($p < 0.0001$) and the overexpressor Δ*vpo*-OE PTS-HAL rescues the hyaluronidase activity of the mutants Δ*vpo* ($p < 0.0001$). Further, Δ*vpo*-OE PTS-HAL is also significantly different from the double-mutant Δ*vpo*-ΔPTS-HAL ($p < 0.0001$).

Fig S3. Pneumococcus attaches to host HA in a process controlled by VP1 and mediated by molecules involved in hyaluronic acid processing.

(A) Spot assay to access attachment to host cells. The wild-type PN4595-T23, and its derivative strains Δ*vp1,* Δ*vp1*:*vp1,* ΔPTS-HAL, Δ*vp1*-ΔPTS-HAL, Δ*vp1*-OE PTS and Δ*hysA*, were assessed for attachment to A549 cells using a spot assay. After washing the unbound bacteria, the total cell-bound bacteria were recovered and plated on TSA plates. (B) Quantification of binding, where the total number of the Δ*vp1*-ΔPTS, Δ*regR and* Δ*hysA,* bound to epithelial cells was enumerated on TSA plates. (C) Measurement of the expression levels of hyaluronic acid synthases-encoding genes *HAS1*, *HAS2*, and *HAS3* in A549 cells at two time points where levels are compared to treatment with a scrambled control. (D) Measurement of the expression levels of hyaluronic acid synthases-encoding genes *HAS2* and *HAS3* after

772 treatment with specific siRNA. (E) Quantification of bacterial binding to A549 pre-incubated
773 with varying concentration of HA. Data on B to E represents the mean ± S.E.M of at least four
774 independent experiments. Statistical significance was calculated using unpaired one-way
775 ANOVA (B, D, and E) analysis with Bonferroni correction, and multiple comparison between
776 samples were performed. * $p < 0.005$, ** $p < 0.0001$, ns = not significant.

777

778 **Fig S4. *vp1* mediates attachment to hyaluronic acid of *Streptococcus equis* via genes in**
779 **the PTS-HAL operon.**

780 (A) hyaluronic acid (HA) coating of 6 well plates under listed treatments, visualized by staining
781 with Alcian Blue 8GX. (B) The PMEN1 strain PN4595-T23 (top panel) was assessed for
782 attachment to hyaluronic acid-coated surfaces in FBS-supplemented DMEM media (A549
783 growth media) or Columbia broth (bacterial growth media). The total cell-bound bacteria were
784 recovered and tested for growth on TSA plates.

REFERENCES

1. Troeger C, Blacker B, Khalil I. Estimates of the global, regional, and national morbidity, mortality, and aetiologies of lower respiratory infections in 195 countries, 1990-2016: a systematic analysis for the Global Burden of Disease Study 2016. Lancet Infect Dis. 2018;18(11):1191–210.

2. Murdoch DR, Howie SRC. The global burden of lower respiratory infections: making progress, but we need to do better. Lancet Infect Dis. 2018;18(11):1162–3.

3. Weiser JN, Ferreira DM, Paton JC. Streptococcus pneumoniae: transmission, colonization and invasion. Nat Rev Microbiol. 2018 Jun;16(6):355–67.

4. Brown AO, Mann B, Gao G, Hankins JS, Humann J, Giardina J, et al. Streptococcus pneumoniae Translocates into the Myocardium and Forms Unique Microlesions That Disrupt Cardiac Function. PLOS Pathog. 2014 Sep 18;10(9):e1004383.

5. Loughran AJ, Orihuela CJ, Tuomanen EI. Streptococcus pneumoniae: Invasion and Inflammation. Microbiol Spectr. 2019;7(2).

6. Aggarwal SD, Eutsey R, West-Roberts J, Domenech A, Xu W, Abdullah IT, et al. Function of BriC peptide in the pneumococcal competence and virulence portfolio. PLoS Pathog [Internet]. 2018 Oct 11 [cited 2019 Jul 29];14(10). Available from: https://www.ncbi.nlm.nih.gov/pmc/articles/PMC6181422/

7. Cuevas RA, Eutsey R, Kadam A, West-Roberts JA, Woolford CA, Mitchell AP, et al. A novel streptococcal cell-cell communication peptide promotes pneumococcal virulence and biofilm formation. Mol Microbiol. 2017 Aug;105(4):554–71.

8. Dawid S, Roche AM, Weiser JN. The blp bacteriocins of Streptococcus pneumoniae mediate intraspecies competition both in vitro and in vivo. Infect Immun. 2007 Jan;75(1):443–51.

9. de Saizieu A, Gardès C, Flint N, Wagner C, Kamber M, Mitchell TJ, et al. Microarray-based identification of a novel Streptococcus pneumoniae regulon controlled by an autoinduced peptide. J Bacteriol. 2000 Sep;182(17):4696–703.

10. Havarstein LS, Coomaraswamy G, Morrison DA. An unmodified heptadecapeptide pheromone induces competence for genetic transformation in Streptococcus pneumoniae. Proc Natl Acad Sci U S A. 1995 Nov 21;92(24):11140–4.

11. Hoover SE, Perez AJ, Tsui H-CT, Sinha D, Smiley DL, DiMarchi RD, et al. A new quorum-sensing system (TprA/PhrA) for Streptococcus pneumoniae D39 that regulates a lantibiotic biosynthesis gene cluster. Mol Microbiol. 2015 Apr 13;

12. Junges R, Salvadori G, Shekhar S, Åmdal HA, Periselneris JN, Chen T, et al. A Quorum-Sensing System That Regulates Streptococcus pneumoniae Biofilm Formation and Surface Polysaccharide Production. mSphere [Internet]. 2017 Sep 13;2(5). Available from: https://www.ncbi.nlm.nih.gov/pmc/articles/PMC5597970/

13. Kadam A, Eutsey RA, Rosch J, Miao X, Longwell M, Xu W, et al. Promiscuous signaling by a regulatory system unique to the pandemic PMEN1 pneumococcal lineage. PLOS Pathog. 2017 May 18;13(5):e1006339.

14. Lux T, Nuhn M, Hakenbeck R, Reichmann P. Diversity of Bacteriocins and Activity Spectrum in Streptococcus pneumoniae. J Bacteriol. 2007 Nov;189(21):7741–51.

15. Motib Anfal, Guerreiro Antonio, Al-Bayati Firas, Piletska Elena, Manzoor Irfan, Shafeeq Sulman, et al. Modulation of Quorum Sensing in a Gram-Positive Pathogen by Linear Molecularly Imprinted Polymers with Anti-infective Properties. Angew Chem. 2017 Nov 30;129(52):16782–5.

16. Motib AS, Al-Bayati FAY, Manzoor I, Shafeeq S, Kadam A, Kuipers OP, et al. TprA/PhrA Quorum Sensing System Has a Major Effect on Pneumococcal Survival in Respiratory Tract and Blood, and Its Activity Is Controlled by CcpA and GlnR. Front Cell Infect Microbiol [Internet]. 2019 [cited 2019 Sep 20];9. Available from: https://www.frontiersin.org/articles/10.3389/fcimb.2019.00326/full

17. Tomasz A. Control of the Competent State in Pneumococcus by a Hormone-Like Cell Product: An Example for a New Type of Regulatory Mechanism in Bacteria. Nature. 1965 Oct 9;208(5006):155–9.

18. Zhi X, Abdullah IT, Gazioglu O, Manzoor I, Shafeeq S, Kuipers OP, et al. Rgg-Shp regulators are important for pneumococcal colonization and invasion through their effect on mannose utilization and capsule synthesis. Sci Rep. 2018 Apr 23;8(1):6369.

19. Havarstein LS, Diep DB, Nes IF. A family of bacteriocin ABC transporters carry out proteolytic processing of their substrates concomitant with export. Mol Microbiol. 1995 Apr 1;16(2):229–40.

20. Aprianto R, Slager J, Holsappel S, Veening J-W. High-resolution analysis of the pneumococcal transcriptome under a wide range of infection-relevant conditions. Nucleic Acids Res. 2018 02;46(19):9990–10006.

21. Hall-Stoodley L, Hu FZ, Gieseke A, Nistico L, Nguyen D, Hayes J, et al. Direct Detection of Bacterial Biofilms on the Middle-Ear Mucosa of Children With Chronic Otitis Media. JAMA J Am Med Assoc. 2006 Jul 12;296(2):202–11.

22. Hoa M, Syamal M, Sachdeva L, Berk R, Coticchia J. Demonstration of nasopharyngeal and middle ear mucosal biofilms in an animal model of acute otitis media. Ann Otol Rhinol Laryngol. 2009 Apr;118(4):292–8.

23. Post JC, Hiller NL, Nistico L, Stoodley P, Ehrlich GD. The role of biofilms in otolaryngologic infections: update 2007. Curr Opin Otolaryngol Head Neck Surg. 2007 Oct;15(5):347–51.

24. Sanderson AR, Leid JG, Hunsaker D. Bacterial biofilms on the sinus mucosa of human subjects with chronic rhinosinusitis. The Laryngoscope. 2006 Jul;116(7):1121–6.

25. Chao Y, Marks LR, Pettigrew MM, Hakansson AP. Streptococcus pneumoniae biofilm formation and dispersion during colonization and disease. Front Cell Infect Microbiol. 2015;4(January):194.

26. Marks LR, Davidson BA, Knight PR, Hakansson AP. Interkingdom Signaling Induces Streptococcus pneumoniae Biofilm Dispersion and Transition from Asymptomatic Colonization to Disease. mBio. 2013;4(4):e00438-13.

27. Chao Y, Marks LR, Pettigrew MM, Hakansson AP. Streptococcus pneumoniae biofilm formation and dispersion during colonization and disease. Front Cell Infect Microbiol. 2014;4:194.

28. Croucher NJ, Harris SR, Barquist L, Parkhill J, Bentley SD. A high-resolution view of genome-wide pneumococcal transformation. PLoS Pathog. 2012;8(6):e1002745.

29. Marks LR, Parameswaran GI, Hakansson AP. Pneumococcal interactions with epithelial cells are crucial for optimal biofilm formation and colonization in vitro and in vivo. Infect Immun. 2012 Aug;80(8):2744–60.

30. Tonnaer EL, Mylanus EA, Mulder JJ, Curfs JH. Detection of bacteria in healthy middle ears during cochlear implantation. Arch Otolaryngol Head Neck Surg. 2009 Mar;135(3):232–7.

31. Trappetti C, Gualdi L, Meola LD, Jain P, Korir CC, Edmonds P, et al. The impact of the competence quorum sensing system on Streptococcus pneumoniae biofilms varies depending on the experimental model. BMC Microbiol. 2011 Apr 14;11(1):75.

32. Vidal JE, Ludewick HP, Kunkel RM, Zähner D, Klugman KP. The LuxS-Dependent Quorum-Sensing System Regulates Early Biofilm Formation by Streptococcus pneumoniae Strain D39 ▿ . Infect Immun. 2011 Oct;79(10):4050–60.

33. Couchman JR, Pataki CA. An Introduction to Proteoglycans and Their Localization. J Histochem Cytochem. 2012 Dec;60(12):885–97.

34. Iozzo RV, Schaefer L. Proteoglycan form and function: A comprehensive nomenclature of proteoglycans. Matrix Biol J Int Soc Matrix Biol. 2015 Mar;42:11–55.

35. Weigel PH, DeAngelis PL. Hyaluronan synthases: a decade-plus of novel glycosyltransferases. J Biol Chem. 2007 Dec 21;282(51):36777–81.

36. Pomin VH, Mulloy B. Glycosaminoglycans and Proteoglycans. Pharmaceuticals [Internet]. 2018 Feb 27 [cited 2019 Sep 3];11(1). Available from: https://www.ncbi.nlm.nih.gov/pmc/articles/PMC5874723/

37. Taylor KR, Gallo RL. Glycosaminoglycans and their proteoglycans: host-associated molecular patterns for initiation and modulation of inflammation. FASEB J Off Publ Fed Am Soc Exp Biol. 2006 Jan;20(1):9–22.

38. Andre GO, Converso TR, Politano WR, Ferraz LFC, Ribeiro ML, Leite LCC, et al. Role of Streptococcus pneumoniae Proteins in Evasion of Complement-Mediated Immunity. Front Microbiol. 2017;8:224.

898 39. Frolet C, Beniazza M, Roux L, Gallet B, Noirclerc-Savoye M, Vernet T, et al. New
899 adhesin functions of surface-exposed pneumococcal proteins. BMC Microbiol. 2010 Jul
900 12;10:190.

901 40. García B, Merayo-Lloves J, Rodríguez D, Alcalde I, García-Suárez O, Alfonso JF, et al.
902 Different Use of Cell Surface Glycosaminoglycans As Adherence Receptors to Corneal
903 Cells by Gram Positive and Gram Negative Pathogens. Front Cell Infect Microbiol.
904 2016;6:173.

905 41. Hammerschmidt S. Adherence molecules of pathogenic pneumococci. Curr Opin
906 Microbiol. 2006 Feb;9(1):12–20.

907 42. Birkenhauer E, Neethirajan S, Weese JS. Collagen and hyaluronan at wound sites
908 influence early polymicrobial biofilm adhesive events. BMC Microbiol. 2014 Jul
909 16;14:191.

910 43. Rajas O, Quirós LM, Ortega M, Vazquez-Espinosa E, Merayo-Lloves J, Vazquez F, et al.
911 Glycosaminoglycans are involved in bacterial adherence to lung cells. BMC Infect Dis.
912 2017 02;17(1):319.

913 44. Bhaskar KR, O'Sullivan DD, Opaskar-Hincman H, Reid LM, Coles SJ. Density gradient
914 analysis of secretions produced in vitro by human and canine airway mucosa:
915 identification of lipids and proteoglycans in such secretions. Exp Lung Res.
916 1986;10(4):401–22.

917 45. Monzon ME, Casalino-Matsuda SM, Forteza RM. Identification of glycosaminoglycans in
918 human airway secretions. Am J Respir Cell Mol Biol. 2006 Feb;34(2):135–41.

919 46. Jiang D, Liang J, Noble PW. Regulation of non-infectious lung injury, inflammation, and
920 repair by the extracellular matrix glycosaminoglycan hyaluronan. Anat Rec Hoboken NJ
921 2007. 2010 Jun;293(6):982–5.

922 47. Jiang D, Liang J, Noble PW. Hyaluronan in tissue injury and repair. Annu Rev Cell Dev
923 Biol. 2007;23:435–61.

924 48. Lennon FE, Singleton PA. Role of hyaluronan and hyaluronan-binding proteins in lung
925 pathobiology. Am J Physiol Lung Cell Mol Physiol. 2011 Aug;301(2):L137-147.

926 49. Kujawa MJ, Caplan AI. Hyaluronic acid bonded to cell-culture surfaces stimulates
927 chondrogenesis in stage 24 limb mesenchyme cell cultures. Dev Biol. 1986
928 Apr;114(2):504–18.

929 50. Nusgens B-V. [Hyaluronic acid and extracellular matrix: a primitive molecule?]. Ann
930 Dermatol Venereol. 2010 Apr;137 Suppl 1:S3-8.

931 51. Solis MA, Chen Y-H, Wong TY, Bittencourt VZ, Lin Y-C, Huang LLH. Hyaluronan
932 regulates cell behavior: a potential niche matrix for stem cells. Biochem Res Int.
933 2012;2012:346972.

52. Bidossi A, Mulas L, Decorosi F, Colomba L, Ricci S, Pozzi G, et al. A functional genomics approach to establish the complement of carbohydrate transporters in Streptococcus pneumoniae. PloS One. 2012;7(3):e33320.

53. Oiki S, Mikami B, Maruyama Y, Murata K, Hashimoto W. A bacterial ABC transporter enables import of mammalian host glycosaminoglycans. Sci Rep. 2017 21;7(1):1069.

54. Chapuy-Regaud S, Ogunniyi AD, Diallo N, Huet Y, Desnottes J-F, Paton JC, et al. RegR, a global LacI/GalR family regulator, modulates virulence and competence in Streptococcus pneumoniae. Infect Immun. 2003 May;71(5):2615–25.

55. Maruyama Y, Nakamichi Y, Itoh T, Mikami B, Hashimoto W, Murata K. Substrate specificity of streptococcal unsaturated glucuronyl hydrolases for sulfated glycosaminoglycan. J Biol Chem. 2009 Jul 3;284(27):18059–69.

56. Marion C, Stewart JM, Tazi MF, Burnaugh AM, Linke CM, Woodiga SA, et al. Streptococcus pneumoniae can utilize multiple sources of hyaluronic acid for growth. Infect Immun. 2012 Apr;80(4):1390–8.

57. Yadav MK, Chae S-W, Park K, Song J-J. Hyaluronic acid derived from other streptococci supports Streptococcus pneumoniae in vitro biofilm formation. BioMed Res Int. 2013;2013:690217.

58. Hendriksen WT, Bootsma HJ, Estevão S, Hoogenboezem T, de Jong A, de Groot R, et al. CodY of Streptococcus pneumoniae: link between nutritional gene regulation and colonization. J Bacteriol. 2008 Jan;190(2):590–601.

59. Croucher NJ, Harris SR, Fraser C, Quail MA, Burton J, van der Linden M, et al. Rapid pneumococcal evolution in response to clinical interventions. Science. 2011 Jan 28;331(6016):430–4.

60. Hiller NL, Eutsey RA, Powell E, Earl JP, Janto B, Martin DP, et al. Differences in Genotype and Virulence among Four Multidrug-Resistant Streptococcus pneumoniae Isolates Belonging to the PMEN1 Clone. PLoS ONE. 2011 Dec 19;6(12):e28850.

61. Nesin M, Ramirez M, Tomasz A. Capsular transformation of a multidrug-resistant Streptococcus pneumoniae in vivo. J Infect Dis. 1998 Mar;177(3):707–713.

62. Wyres KL, Lambertsen LM, Croucher NJ, McGee L, von Gottberg A, Liñares J, et al. Pneumococcal capsular switching: a historical perspective. J Infect Dis. 2013 Feb 1;207(3):439–49.

63. Tettelin H, Nelson KE, Paulsen IT, Eisen JA, Read TD, Peterson S, et al. Complete genome sequence of a virulent isolate of Streptococcus pneumoniae. Science. 2001 Jul 20;293(5529):498–506.

64. Brittan JL, Buckeridge TJ, Finn A, Kadioglu A, Jenkinson HF. Pneumococcal neuraminidase A: an essential upper airway colonization factor for Streptococcus pneumoniae. Mol Oral Microbiol. 2012 Aug;27(4):270–83.

971 65. Kjos M, Aprianto R, Fernandes VE, Andrew PW, van Strijp JAG, Nijland R, et al. Bright
972 fluorescent Streptococcus pneumoniae for live-cell imaging of host-pathogen
973 interactions. J Bacteriol. 2015 Mar;197(5):807–18.

974 66. Balis JU, Bumgarner SD, Paciga JE, Paterson JF, Shelley SA. Synthesis of lung
975 surfactant-associated glycoproteins by A549 cells: description of an in vitro model for
976 human type II cell dysfunction. Exp Lung Res. 1984;6(3–4):197–213.

977 67. Lieber M, Smith B, Szakal A, Nelson-Rees W, Todaro G. A continuous tumor-cell line
978 from a human lung carcinoma with properties of type II alveolar epithelial cells. Int J
979 Cancer. 1976 Jan 15;17(1):62–70.

980 68. Nardone LL, Andrews SB. Cell line A549 as a model of the type II pneumocyte.
981 Phospholipid biosynthesis from native and organometallic precursors. Biochim Biophys
982 Acta. 1979 May 25;573(2):276–95.

983 69. Berger JT, Voynow JA, Peters KW, Rose MC. Respiratory carcinoma cell lines. MUC
984 genes and glycoconjugates. Am J Respir Cell Mol Biol. 1999 Mar;20(3):500–10.

985 70. Carterson AJ, Höner zu Bentrup K, Ott CM, Clarke MS, Pierson DL, Vanderburg CR, et
986 al. A549 lung epithelial cells grown as three-dimensional aggregates: alternative tissue
987 culture model for Pseudomonas aeruginosa pathogenesis. Infect Immun. 2005
988 Feb;73(2):1129–40.

989 71. Raffel FK, Szelestey BR, Beatty WL, Mason KM. The Haemophilus influenzae Sap
990 transporter mediates bacterium-epithelial cell homeostasis. Infect Immun.
991 2013;81(1):43–54.

992 72. Cook LC, Federle MJ. Peptide pheromone signaling in Streptococcus and Enterococcus.
993 FEMS Microbiol Rev. 2014 May;38(3):473–92.

994 73. Martin R, Larsen AH, Corey RA, Midtgaard SR, Frielinghaus H, Schaffitzel C, et al.
995 Structure and Dynamics of the Central Lipid Pool and Proteins of the Bacterial Holo-
996 Translocon. Biophys J. 2019 May 21;116(10):1931–40.

997 74. Kelley LA, Mezulis S, Yates CM, Wass MN, Sternberg MJE. The Phyre2 web portal for
998 protein modeling, prediction and analysis. Nat Protoc. 2015 Jun;10(6).

999 75. Dong W, Lu W, McKeehan WL, Luo Y, Ye S. Structural basis of heparan sulfate-specific
000 degradation by heparinase III. Protein Cell. 2012 Dec;3(12):950–61.

001 76. Ma K, Cao Q, Luo S, Wang Z, Liu G, Lu C, et al. cas9 Enhances Bacterial Virulence by
002 Repressing the regR Transcriptional Regulator in Streptococcus agalactiae. Infect
003 Immun. 2018;86(3).

004 77. Reese MG. Application of a time-delay neural network to promoter annotation in the
005 Drosophila melanogaster genome. Comput Chem. 2001 Dec;26(1):51–6.

006 78. Solovyev V, Salamov A. Automatic Annotation of Microbial Genomes and Metagenomic
007 Sequences. In Metagenomics and its Applications in Agriculture, Biomedicine and
008 Environmental Studies. Nova Science Publisher; 2011. 61–78 p.

009 79. Takao A. Cloning and expression of hyaluronate lyase genes of Streptococcus
010 intermedius and Streptococcus constellatus subsp. constellatus(1). FEMS Microbiol Lett.
011 2003 Feb 14;219(1):143–50.

012 80. Sung CK, Li H, Claverys JP, Morrison DA. An rpsL Cassette, Janus, for Gene
013 Replacement through Negative Selection in Streptococcus pneumoniae. Appl Environ
014 Microbiol. 2001 Nov;67(11):5190–6.

015 81. Wang T, Cui Y, Jin J, Guo J, Wang G, Yin X, et al. Translating mRNAs strongly correlate
016 to proteins in a multivariate manner and their translation ratios are phenotype specific.
017 Nucleic Acids Res. 2013 May;41(9):4743–54.

018 82. Chow G, Tauler J, Mulshine JL. Cytokines and growth factors stimulate hyaluronan
019 production: role of hyaluronan in epithelial to mesenchymal-like transition in non-small
020 cell lung cancer. J Biomed Biotechnol. 2010;2010:485468.

021 83. Glanville DG, Han L, Maule AF, Woodacre A, Thanki D, Abdullah IT, et al. RitR is an
022 archetype for a novel family of redox sensors in the streptococci that has evolved from
023 two-component response regulators and is required for pneumococcal colonization.
024 PLoS Pathog. 2018;14(5):e1007052.

025 84. Kahya HF, Andrew PW, Yesilkaya H. Deacetylation of sialic acid by esterases
026 potentiates pneumococcal neuraminidase activity for mucin utilization, colonization and
027 virulence. PLOS Pathog. 2017 Mar 3;13(3):e1006263.

028 85. Bogaert D, de Groot R, Hermans P. Streptococcus pneumoniae colonisation: the key to
029 pneumococcal disease. Lancet Infect Dis. 2004 Mar;4(3):144–54.

030 86. Kadioglu A, Weiser JN, Paton JC, Andrew PW. The role of Streptococcus pneumoniae
031 virulence factors in host respiratory colonization and disease. Nat Rev Microbiol. 2008
032 Apr;6(4):288–301.

033 87. Hendriksen WT, Bootsma HJ, Estevão S, Hoogenboezem T, de Jong A, de Groot R, et
034 al. CodY of Streptococcus pneumoniae: link between nutritional gene regulation and
035 colonization. J Bacteriol. 2008 Jan;190(2):590–601.

036 88. Lysenko ES, Lijek RS, Brown SP, Weiser JN. Within-host competition drives selection for
037 the capsule virulence determinant of Streptococcus pneumoniae. Curr Biol CB. 2010 Jul
038 13;20(13):1222–6.

039 89. Bergmann S, Hammerschmidt S. Versatility of pneumococcal surface proteins.
040 Microbiology. 2006 Feb 1;152(2):295–303.

041 90. Paterson GK, Orihuela CJ. Pneumococcal microbial surface components recognizing
042 adhesive matrix molecules targeting of the extracellular matrix. Mol Microbiol. 2010 Jul
043 1;77(1):1–5.

044 91. Jensch I, Gámez G, Rothe M, Ebert S, Fulde M, Somplatzki D, et al. PavB is a surface-
045 exposed adhesin of Streptococcus pneumoniae contributing to nasopharyngeal
046 colonization and airways infections. Mol Microbiol. 2010 Jul 1;77(1):22–43.

047 92. Kanwal S, Jensch I, Palm GJ, Brönstrup M, Rohde M, Kohler TP, et al. Mapping the
048 recognition domains of pneumococcal fibronectin-binding proteins PavA and PavB
049 demonstrates a common pattern of molecular interactions with fibronectin type III
050 repeats. Mol Microbiol. 2017 Sep;105(6):839–59.

051 93. Pracht D, Elm C, Gerber J, Bergmann S, Rohde M, Seiler M, et al. PavA of
052 Streptococcus pneumoniae modulates adherence, invasion, and meningeal
053 inflammation. Infect Immun. 2005 May;73(5):2680–9.

054 94. Antikainen J, Kuparinen V, Lähteenmäki K, Korhonen TK. Enolases from Gram-positive
055 bacterial pathogens and commensal lactobacilli share functional similarity in virulence-
056 associated traits. FEMS Immunol Med Microbiol. 2007 Dec;51(3):526–34.

057 95. Bergmann S, Rohde M, Chhatwal GS, Hammerschmidt S. alpha-Enolase of
058 Streptococcus pneumoniae is a plasmin(ogen)-binding protein displayed on the bacterial
059 cell surface. Mol Microbiol. 2001 Jun;40(6):1273–87.

060 96. Papasergi S, Garibaldi M, Tuscano G, Signorino G, Ricci S, Peppoloni S, et al.
061 Plasminogen- and fibronectin-binding protein B is involved in the adherence of
062 Streptococcus pneumoniae to human epithelial cells. J Biol Chem. 2010 Mar
063 5;285(10):7517–24.

064 97. Yamaguchi M, Terao Y, Mori Y, Hamada S, Kawabata S. PfbA, a novel plasmin- and
065 fibronectin-binding protein of Streptococcus pneumoniae, contributes to fibronectin-
066 dependent adhesion and antiphagocytosis. J Biol Chem. 2008 Dec 26;283(52):36272–9.

067 98. Voss S, Hallström T, Saleh M, Burchhardt G, Pribyl T, Singh B, et al. The choline-binding
068 protein PspC of Streptococcus pneumoniae interacts with the C-terminal heparin-binding
069 domain of vitronectin. J Biol Chem. 2013 May 31;288(22):15614–27.

070 99. Shivshankar P, Sanchez C, Rose LF, Orihuela CJ. The Streptococcus pneumoniae
071 adhesin PsrP binds to Keratin 10 on lung cells. Mol Microbiol. 2009 Aug;73(4):663–79.

072 100. King SJ, Hippe KR, Weiser JN. Deglycosylation of human glycoconjugates by the
073 sequential activities of exoglycosidases expressed by Streptococcus pneumoniae. Mol
074 Microbiol. 2006 Feb;59(3):961–74.

075 101. Limoli DH, Sladek JA, Fuller LA, Singh AK, King SJ. BgaA acts as an adhesin to mediate
076 attachment of some pneumococcal strains to human epithelial cells. Microbiol Read
077 Engl. 2011 Aug;157(Pt 8):2369–81.

078 102. Singh AK, Pluvinage B, Higgins MA, Dalia AB, Woodiga SA, Flynn M, et al. Unravelling
079 the multiple functions of the architecturally intricate Streptococcus pneumoniae β-
080 galactosidase, BgaA. PLoS Pathog. 2014 Sep;10(9):e1004364.

081 103. Warner JB, Lolkema JS. CcpA-dependent carbon catabolite repression in bacteria.
082 Microbiol Mol Biol Rev MMBR. 2003 Dec;67(4):475–90.

083 104. Carvalho SM, Kloosterman TG, Kuipers OP, Neves AR. CcpA Ensures Optimal
084 Metabolic Fitness of Streptococcus pneumoniae. PLoS ONE. 2011 Oct 21;6(10):e26707.

085 105. Corradetti B, Taraballi F, Martinez JO, Minardi S, Basu N, Bauza G, et al. Hyaluronic
086 acid coatings as a simple and efficient approach to improve MSC homing toward the site
087 of inflammation. Sci Rep. 2017 11;7(1):7991.

088 106. Khademhosseini A, Suh KY, Yang JM, Eng G, Yeh J, Levenberg S, et al. Layer-by-layer
089 deposition of hyaluronic acid and poly-L-lysine for patterned cell co-cultures.
090 Biomaterials. 2004 Aug;25(17):3583–92.

091 107. Aoki K, Matsumoto S, Hirayama Y, Wada T, Ozeki Y, Niki M, et al. Extracellular
092 mycobacterial DNA-binding protein 1 participates in mycobacterium-lung epithelial cell
093 interaction through hyaluronic acid. J Biol Chem. 2004 Sep 17;279(38):39798–806.

094 108. Aaberge IS, Eng J, Lermark G, Løvik M. Virulence of Streptococcus pneumoniae in mice:
095 a standardized method for preparation and frozen storage of the experimental bacterial
096 inoculum. Microb Pathog. 1995 Feb;18(2):141–52.

097 109. Huang H. Design and Characterization of Artificial Transcriptional Terminators.
098 Massachusetts Institute of Technology; 2008.

099 110. Kadam A, Janto B, Eutsey R, Earl JP, Powell E, Dahlgren ME, et al. Streptococcus
100 pneumoniae Supragenome Hybridization Arrays for Profiling of Genetic Content and
101 Gene Expression. Curr Protoc Microbiol. 2015;36:9D.4.1-9D.4.20.

102 111. Kayala MA, Baldi P. Cyber-T web server: differential analysis of high-throughput data.
103 Nucleic Acids Res. 2012 Jul;40(Web Server issue):W553-559.

104 112. Horta CCR, Magalhães B de F, Oliveira-Mendes BBR, do Carmo AO, Duarte CG,
105 Felicori LF, et al. Molecular, Immunological, and Biological Characterization of Tityus
106 serrulatus Venom Hyaluronidase: New Insights into Its Role in Envenomation. PLoS
107 Negl Trop Dis [Internet]. 2014 Feb 13 [cited 2019 Sep 20];8(2). Available from:
108 https://www.ncbi.nlm.nih.gov/pmc/articles/PMC3923731/

109

110
111

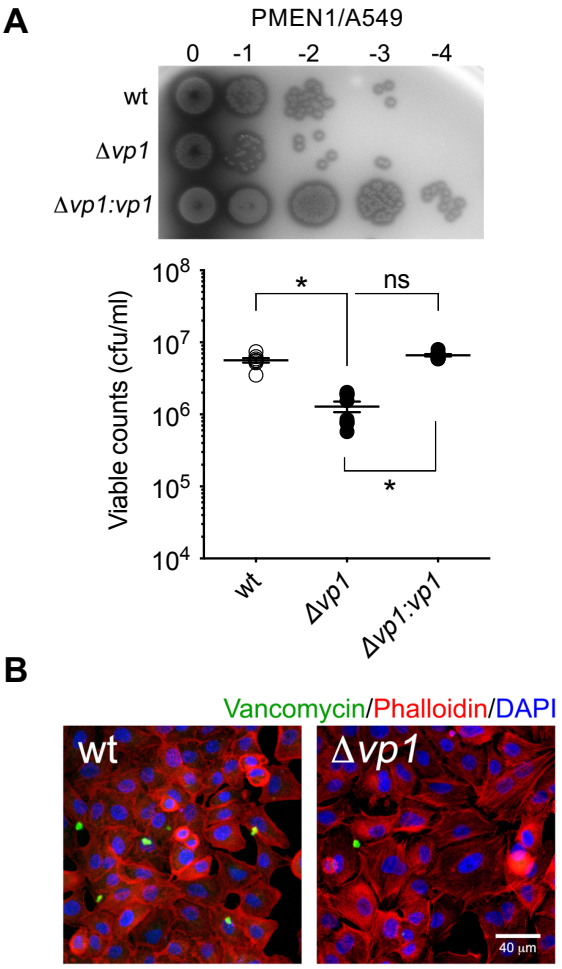

Fig 1. *vp1* enhances pneumococcal attachment to epithelial cells.

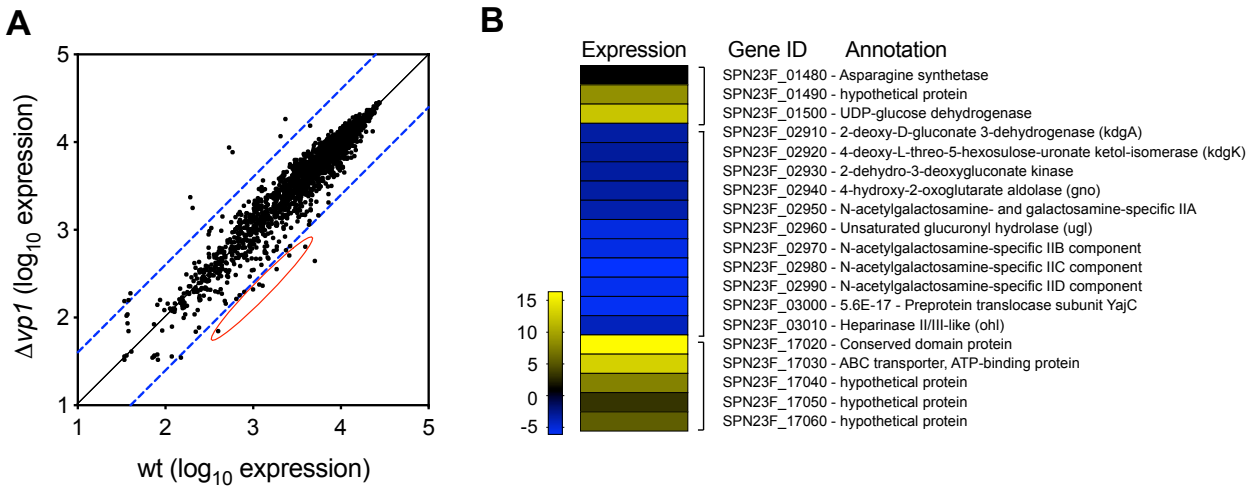

Fig 2. The *vp1* product positively regulates the expression of an operon critical to processing of hyaluronic acid.

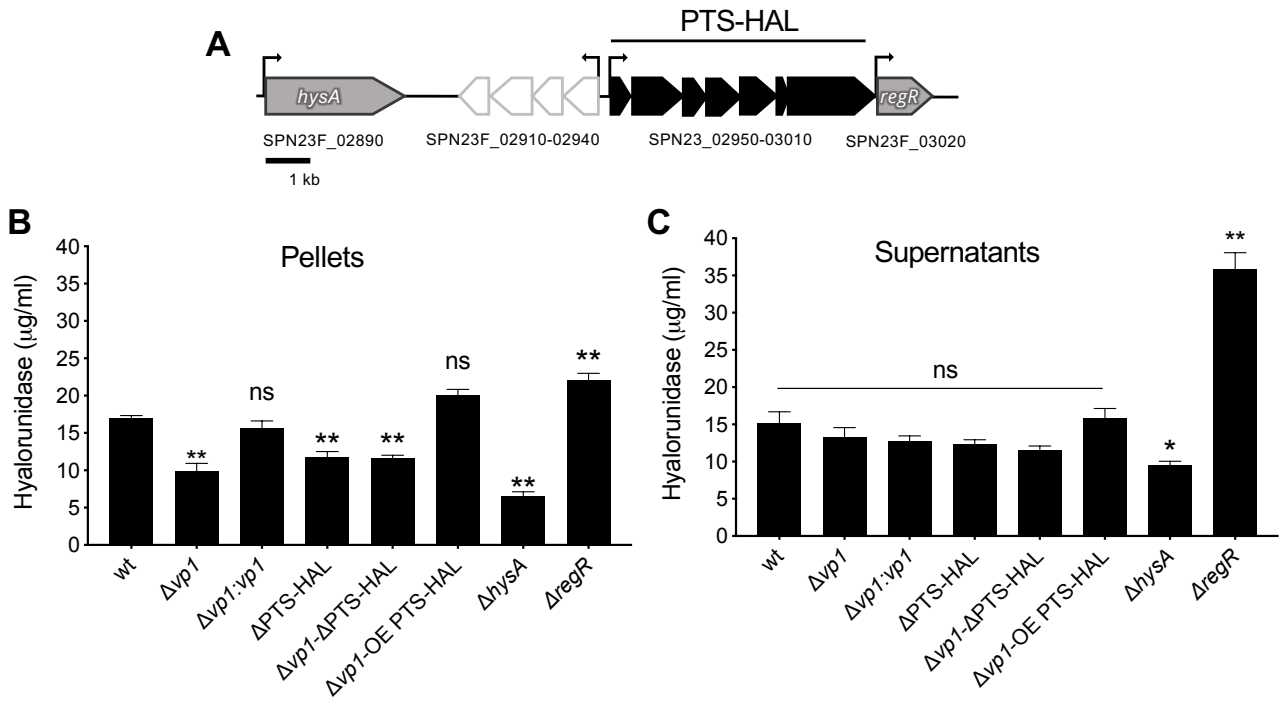

Fig 3. The *vp1* product promotes degradation of the hyaluronan polymer via its controls of the operon encoding the PTS-EII system.

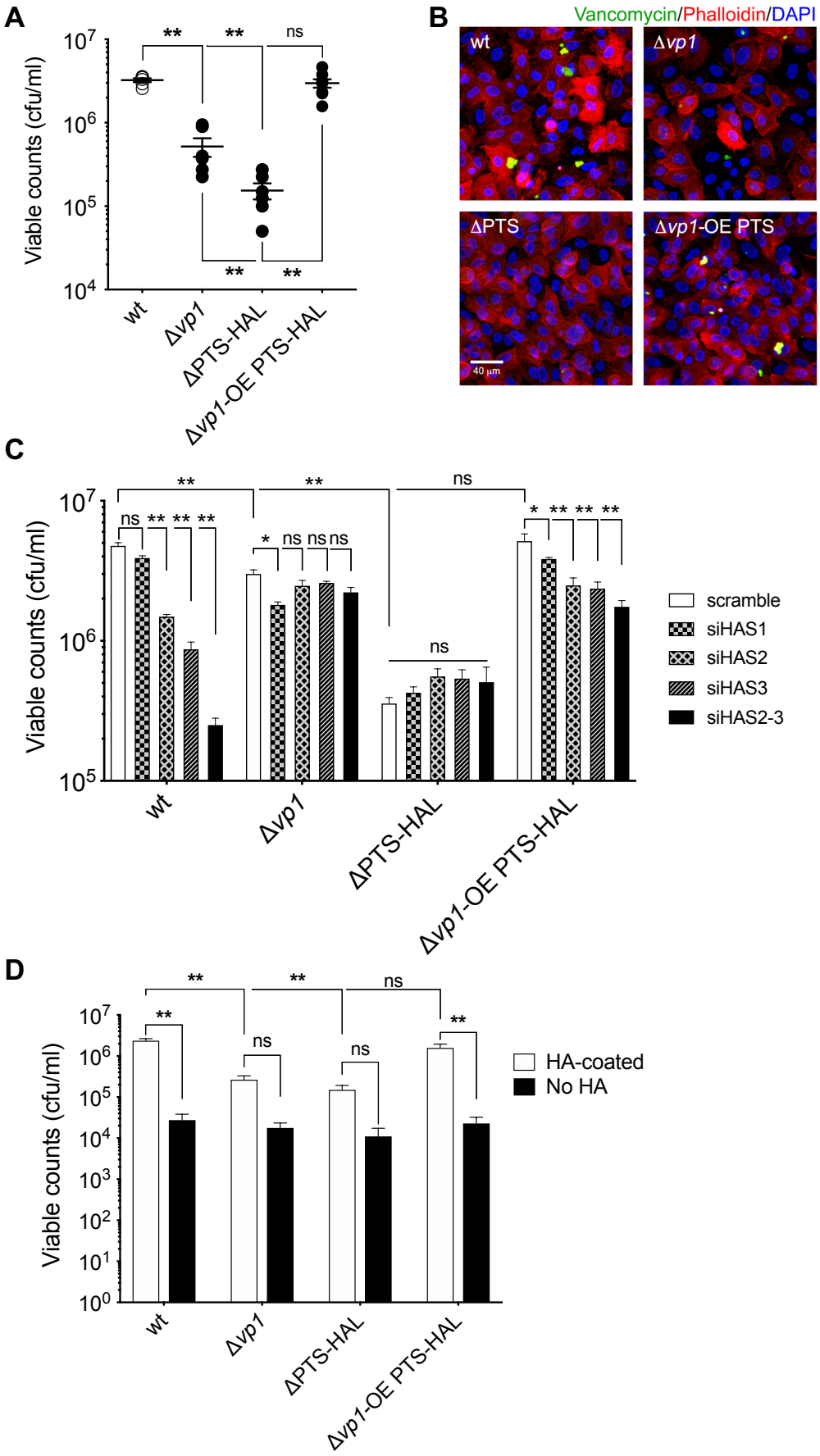

Fig 4. Pneumococcus attaches to host HA in a process controlled by VP1 and mediated by molecules involved in HA processing.

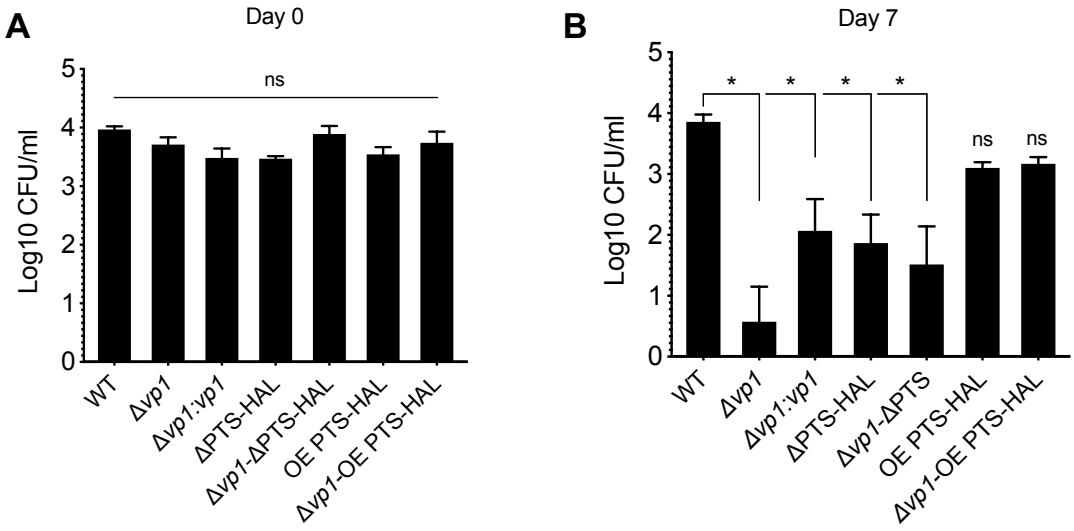

Fig 5. HA processing region is required for pneumococcal colonization.

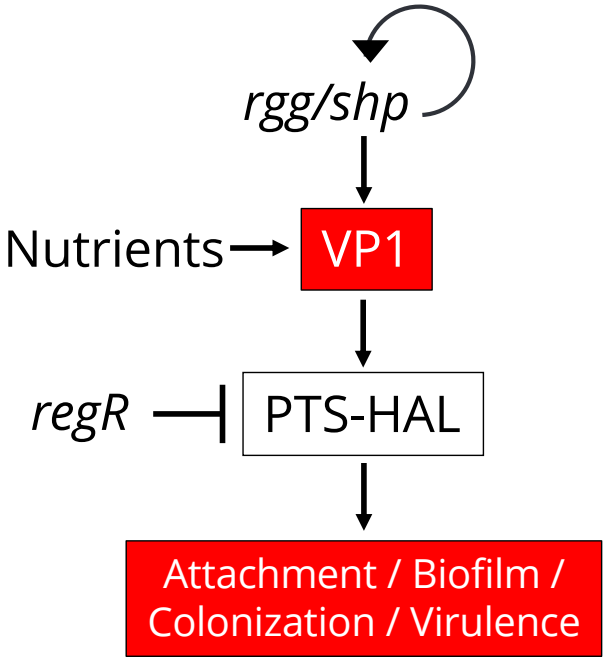

Fig 6. Working model for VP1 regulation and its role in cell-cell communication in *Streptococcus pneumoniae*.

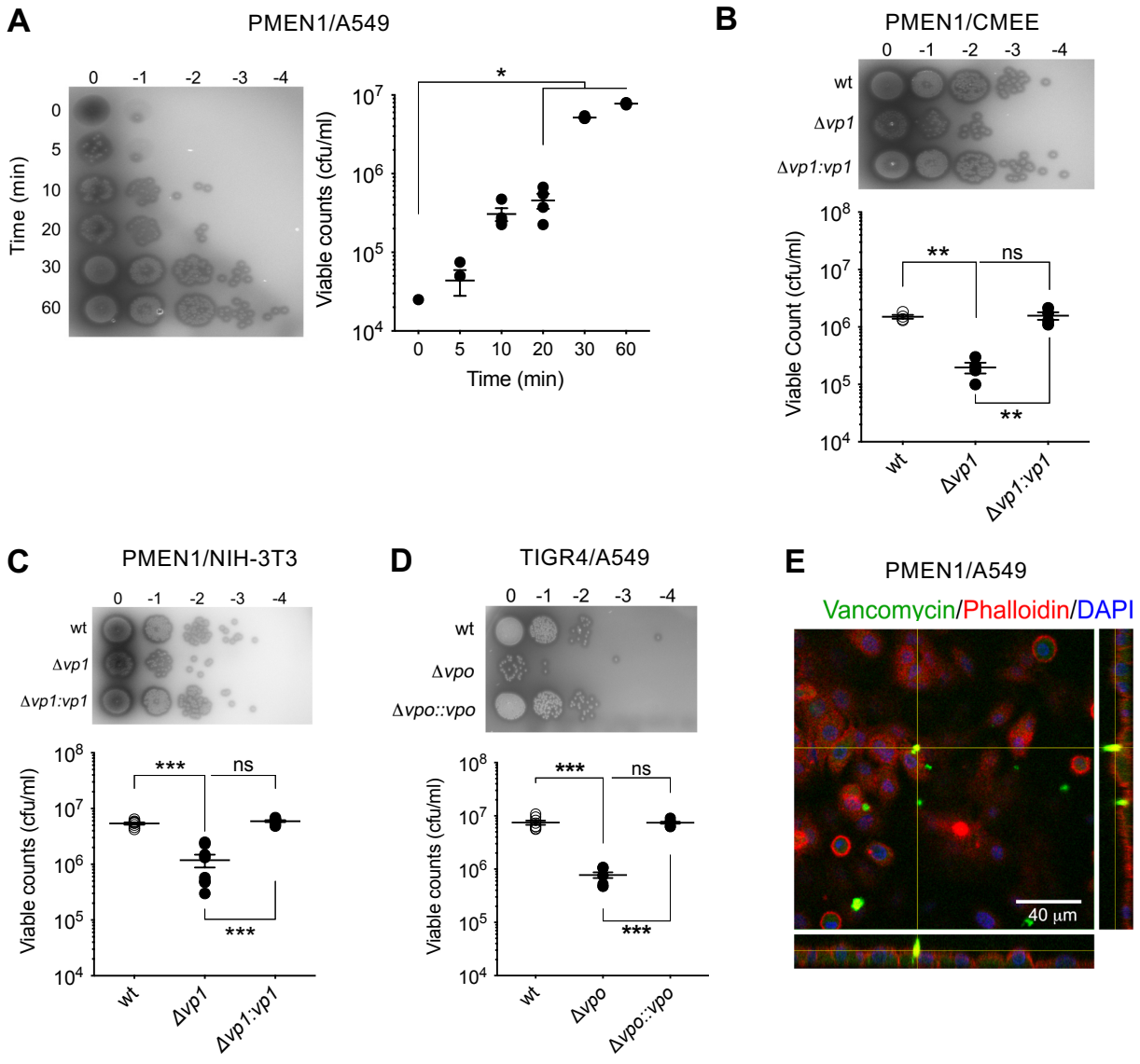

Fig S1. *vp1* enhances pneumococcal attachment to epithelial cells.

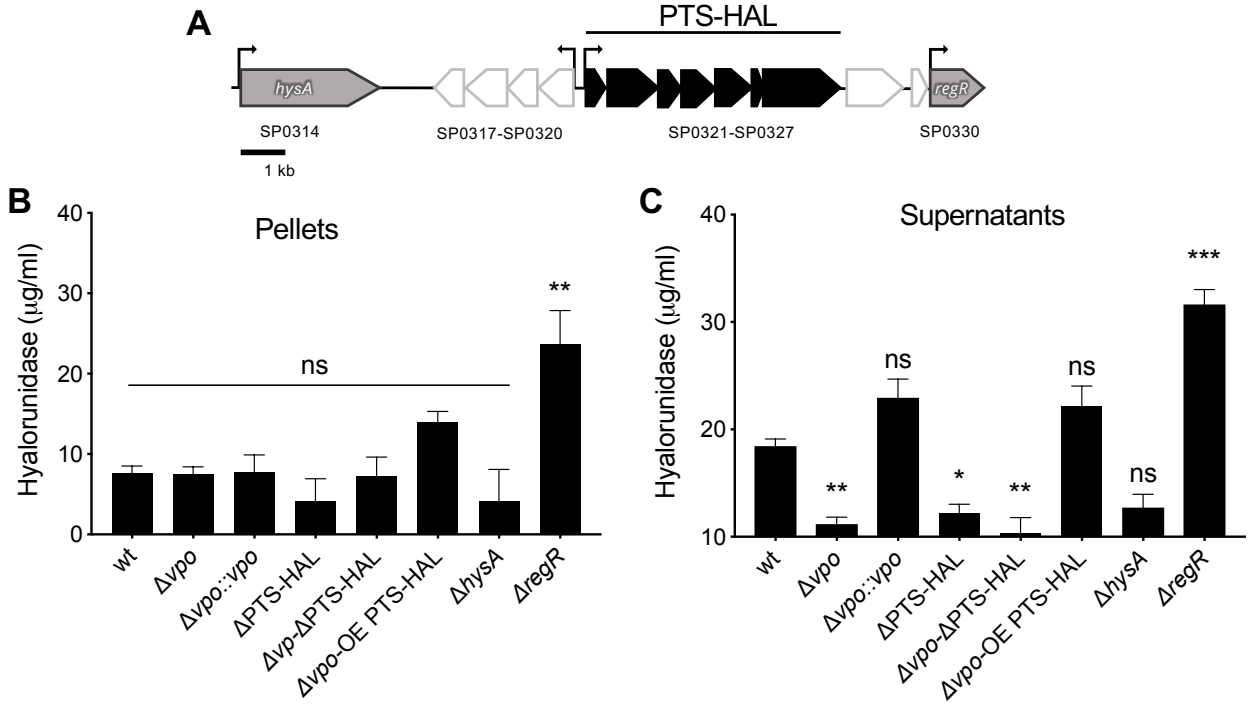

Fig S2. The *vp1* product promotes degradation of the hyaluronan polymer via its controls of the operon encoding the PTS-EII system in TIGR4.

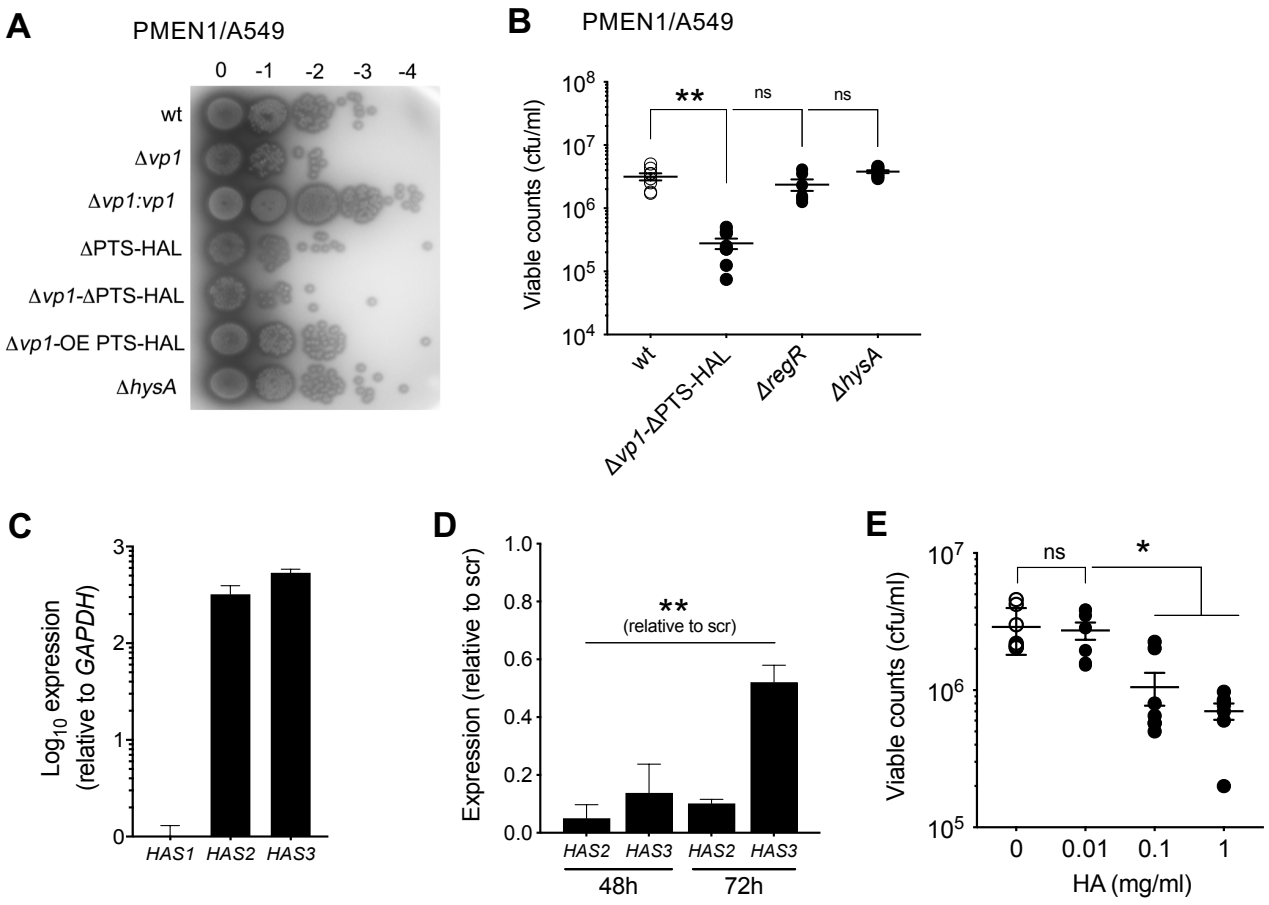

Fig S3. Pneumococcus attaches to host HA in a process controlled by VP1 and mediated by molecules involved in hyaluronic acid processing.

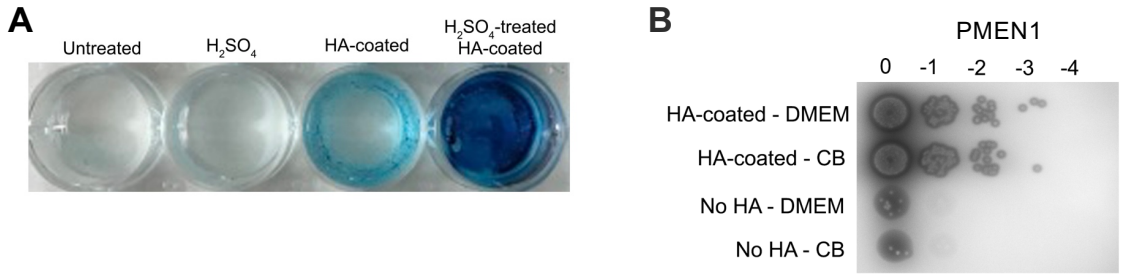

Fig S4. *vp1* mediates attachment to hyaluronic acid of *Streptococcus equis* via genes in the PTS-HAL operon.